

# Autologous multiantigen-targeted T cell therapy for pancreatic cancer: a phase 1/2 trial

---

Received: 16 May 2025

---

Accepted: 30 September 2025

---

Published online: 2 January 2026

---

 Check for updates

---

Benjamin L. Musher<sup>1,2</sup>✉, Spyridoula Vasileiou<sup>1,2</sup>, Brandon G. Smaglo<sup>1,2</sup>, Catherine S. Robertson<sup>1</sup>, Mengfen Wu<sup>1</sup>, Tao Wang<sup>1</sup>, Ayumi Watanabe<sup>1</sup>, Manik Kuvalekar<sup>1</sup>, Yovana Velazquez<sup>1</sup>, Shamika Ketkar<sup>1</sup>, Tamadar Al Doheyan<sup>1</sup>, Penelope G. Papayanni<sup>1</sup>, Aakash Shah<sup>1</sup>, Natalia Lapteva<sup>1</sup>, Bambi J. Grilley<sup>1</sup>, George Van Buren<sup>1</sup>, Premal D. Lulla<sup>1</sup>, Helen E. Heslop<sup>1</sup>, Cliona M. Rooney<sup>1</sup>, Malcolm K. Brenner<sup>1</sup> & Ann M. Leen<sup>1</sup>✉

T cell therapy has proven challenging for pancreatic ductal adenocarcinoma (PDAC), partly due to heterogeneous expression of tumor-associated antigens (TAAs). To address tumor heterogeneity and mitigate immune evasion, an ex vivo expanded, polyclonal, T helper 1 cell-polarized T cell product targeting five TAAs—PRAME, SSX2, MAGEA4, Survivin and NY-ESO-1—was developed. These antigens were chosen based on their tumor specificity, oncogenicity, immunogenicity and level of expression. In a phase 1/2 trial, this autologous nonengineered T cell product was administered ( $1 \times 10^7$  cells  $m^{-2}$  per infusion) monthly to patients with advanced PDAC responding (arm A,  $n = 13$ ) or refractory (arm B,  $n = 12$ ) to first-line chemotherapy or with resectable disease (arm C,  $n = 12$ ). Primary endpoints were safety and feasibility of completing six infusions, whereas exploratory efficacy endpoints included persistence and evaluating the relationship between clinical benefit and the expansion of the infused effector T cells, as well as the induction of de novo immune responses. Of 56 participants procured, 37 were infused, with only 1 treatment-related serious adverse event. Disease control rates in arms A and B were 84.6% (95% confidence interval: 54.6–98.1%) and 25% (95% confidence interval: 5.5–57.2%), respectively. In arm C, two of nine resected participants remained disease free after 66 months of follow-up. The infused cells persisted up to 12 months posttreatment and elevated levels of tumor-directed T cells were detected during dosing ( $P = 0.027$ ) and follow-up in responders compared to nonresponders. Clinical outcomes correlated with peripheral expansion of functional TAA-targeted T cell clones and treatment-emergent antigen spreading. Thus, further investigation of this approach, either as a single agent or combined with other complementary modalities, is warranted (ClinicalTrials.gov identifier: [NCT03192462](https://clinicaltrials.gov/ct2/show/study/NCT03192462)).

Immunotherapies have improved survival in an ever-widening range of malignancies, but eliciting effective antitumor T cell immune responses in patients with pancreatic ductal adenocarcinoma (PDAC), currently the third leading cause of cancer-related death in the USA<sup>1–3</sup>, has proven particularly challenging<sup>4–11</sup>. Multiple factors contribute to PDAC resistance to immunotherapy, including weak expression of target antigens and frequent production or upregulation of immunosuppressive molecules, resulting in a ‘cold’ tumor microenvironment (TME)<sup>12–17</sup>. Even when targetable antigens are present, heterogeneous expression can lead to rapid adaptation and target antigen modulation, which thwart the antitumor potential of T cell monotherapies.

To address tumor heterogeneity and immune evasion, we devised an ex vivo expanded, polyclonal (CD4<sup>+</sup> and CD8<sup>+</sup>), T helper 1 (T<sub>H</sub>1) cell-polarized T cell product targeting a spectrum of tumor-associated antigens (TAAs) using professional antigen-presenting cells and a combination of peptide libraries spanning overexpressed cancer antigens<sup>18</sup>. When administered to patients with hematological malignancies without lymphodepleting chemotherapy (to allow for the recruitment of the endogenous immune system), this platform was previously shown to be safe and associated with the induction of effector immune activity and clinical benefit, including durable tumor control<sup>19–23</sup>.

We postulated that the preparation of a multi-antigen (nonengineered) T cell product specific for PRAME, SSX2, MAGEA4, NY-ESO-1 and Survivin–TAAs chosen based on their tumor specificity, oncogenicity, immunogenicity and level of expression<sup>24–36</sup>—would be feasible, even in heavily pre-treated patients and that infusion of the T cell product would be safe. Additional hypotheses were that these autologous T cells would persist in vivo and that clinical benefit would be associated with the expansion and persistence of the infused effector T cells, as well as the induction of de novo immune responses. We now report the results of TACTOPS, a three-arm, nonrandomized, phase 1/2 clinical trial for patients with PDAC.

## Results

### Patient characteristics

Between 31 January 2018 and 19 December 2019, 56 patients with biopsy-proven PDAC were enrolled and underwent procurement. Multi-antigen T cell (mTAA) manufacturing was successful in all but one case, in which the yield of antigen-presenting cells (dendritic cells (DCs)) was insufficient. Of the remaining enrollees, 18 were not infused due to inability to schedule ( $n = 1$ ), change in eligibility ( $n = 2$ ) and death from progressive PDAC ( $n = 15$ ; in one of these cases, manufacture was consequently halted) (Fig. 1a). Some 37 participants (median age 63 years) were infused with mTAA T cells. Table 1 and Extended Data Table 1 summarize the baseline characteristics of those

who underwent at least one T cell infusion. Patients were enrolled in one of three study arms and could receive up to six infusions. At baseline, patients in arm A had stage III or IV disease ( $n = 2$  (15.4%) or  $n = 11$  (84.6%), respectively), which was either stable or responding to at least 3 months of chemotherapy. Patients in arm B had stage III or IV disease ( $n = 2$  (16.7%) or  $n = 10$  (83.3%), respectively) that had progressed after chemotherapy. All patients in arm C had potentially resectable disease and received their initial T cell infusion between neoadjuvant therapy and planned surgery. At the time of surgery, three participants were unresectable, whereas nine were resected and eight of those received T cells postoperatively.

### Preparation of mTAA T cells: expansion, phenotype, gene profile and functional specificity

T cells underwent a median of 3 (range 2–4) rounds of in vitro stimulation with pepmix-loaded DCs for an average of 24.5 d ( $\pm 0.5$  d) in culture, resulting in a mean 12.5  $\pm$  0.9 fold increase in bulk T cells (Fig. 1b) and yielding sufficient cells for a median of 9 infusions (range 1–28) (Supplementary Table 1). The expanded cells, which were almost exclusively CD3<sup>+</sup> T cells (mean  $\pm$  s.e.m.: 95.7  $\pm$  1.2%), with a mixture of CD4<sup>+</sup> (47.4  $\pm$  3.5%) and CD8<sup>+</sup> (39.0  $\pm$  3.1%) subsets expressing central (CD45RO<sup>+</sup>/CD62L<sup>+</sup>: 14.7  $\pm$  1.9%) and effector memory markers (CD45RO<sup>+</sup>/CD62L<sup>-</sup>: 66.3  $\pm$  2.6%), had an activated phenotype, as evidenced by upregulation of CD69<sup>+</sup> (46.3  $\pm$  2.2%). Naive T (T<sub>naive</sub>) cell, 1.4  $\pm$  0.5% or terminally differentiated T (T<sub>emra</sub>) cell, 2.9  $\pm$  0.7% content was negligible in the final product and the cells were not exhausted (programmed cell death-1 (PD-1; 16.9  $\pm$  1.9%) and lymphocyte activation gene-3 (0.9  $\pm$  0.2%)) (Fig. 1c). Product polyclonality was evaluated by co-staining CD3<sup>+</sup> T cells with an antibody panel covering ~70% of the human T cell receptor (TCR)  $\nu\beta$  repertoire and, as shown in Fig. 1d, all represented  $\nu\beta$  families were detected (mean frequency of 0.2–6.4%,  $n = 25$ ). For more in-depth clonality analysis, TCR complementary determining region 3 (CDR3), deep sequencing was performed on 17 cell lines, in which the presence of a median of 3,375 individual clonotypes (range, 559–10,149) was identified (Fig. 1e, left). Of these, 73.2% (median; range, 44.2–92.9%; Fig. 1e, right) were uniquely identified in the ex vivo expanded product and not in matched patient peripheral blood samples before infusion, thus enabling in vivo tracking of the infused (nongenetically modified) product over time to evaluate persistence.

Transcriptomic characteristics were explored in a subset of antigen-stimulated (versus unstimulated) mTAA T cell products ( $n = 7$ ) by single-cell RNA sequencing (scRNA-seq). Supplementary Fig. 1 shows individual volcano plots with differentially expressed genes (DEGs) (Supplementary Fig. 1a), whereas genes that were upregulated or downregulated in at least three lines are presented in Supplementary Fig. 1b,c. Upregulated genes included those synonymous with migratory

### Fig. 1 | Patient distribution and mTAA T cell characterization studies.

**a**, CONSORT diagram depicting patients enrolled and treated in the three study arms. **b, c**, Fold expansion (**b**) and surface phenotype (**c**, left) and memory (**c**, middle) or activation profile (**c**, right) of mTAA T cells after three cycles of in vitro stimulation (mean  $\pm$  s.e.m.,  $n = 54$  individual patient T cell products). Box plots show the median and 25th and 75th data quartiles. Whiskers extend to the 2.5th and 97.5th percentiles, capturing the lower and upper tails, respectively, of the data distribution. Minima and maxima are plotted. **d**, Clonal diversity evaluated as the mean ( $\pm$ s.e.m.) frequency of mTAA T cells expressing each of the 24 TCR $\nu\beta$  families tested ( $n = 25$  T cell products). Individual data points are overlaid. **e**, Total number of individual TCR clonotypes (left) and proportion of clonotypes unique to the infusion product (not detectable in patient peripheral blood before infusion (right), as assessed by TCR $\nu\beta$  deep sequencing). Each symbol represents an individual patient’s mTAA T cell line ( $n = 17$ ). **f**, Representative scRNA-seq data for patient nos. 12 (left) and 25 (right) showing Uniform Manifold Approximation and Projections of TAA-specific IFN $\gamma$ -expressing cells (top) and dot plots (bottom) for expression of IFN $\gamma$ , PRF1, TNF and GZMB in TAA-stimulated and unstimulated cells. **g**, Detection of IFN $\gamma$ -producing CD4<sup>+</sup> and CD8<sup>+</sup> T cells by ICS. Top: representative donor.

Bottom: summary data (mean  $\pm$  s.e.m.,  $n = 16$  T cell products). **h–j**, Functional capacity of mTAA T cells evaluated within the CD4<sup>+</sup> and CD8<sup>+</sup> compartments by antigen-driven production of effector molecules (**h**); TNF), upregulation of co-stimulatory molecules (**i**; 4-1BB) and degranulation markers (**j**; CD107a). Representative donor examples are shown at the top whereas summary results are shown at the bottom (mean  $\pm$  s.e.m.,  $n = 16$  T cell products). **k**, IFN $\gamma$  ELISpot analysis ( $n = 54$  T cell products). The results are shown as SFCs per  $2 \times 10^5$  input cells (mean  $\pm$  s.e.m.). **l**, Cytolytic potential of mTAA T cells as demonstrated by granzyme B production evaluated by ELISpot ( $n = 16$  T cell products (mean  $\pm$  s.e.m.); individual data points are overlaid). **m**, Specific killing of TAA-loaded autologous targets as measured in a carboxyfluorescein diacetatesuccinimidyl ester (CFSE)-based flow cytometric assay ( $n = 16$  T cell products). The box plots show the median and 25th and 75th data quartiles. The whiskers extend to minima and maxima, capturing the full range of the data. **n**, Lack of cytolytic activity of mTAA T cells against antigen-unloaded autologous targets as assessed in a standard 4-h <sup>51</sup>Cr release assay at the 20:1 E-to-T ratio. Each symbol represents an individual patient’s T cell product ( $n = 54$ ). <sup>a</sup>In one patient who died, product manufacture was halted as a consequence. Mix, Mixture; Neg, Negative; T<sub>cm</sub>, central memory T cell; T<sub>em</sub>, effector memory T cell.; Seq, patient sequence ID.

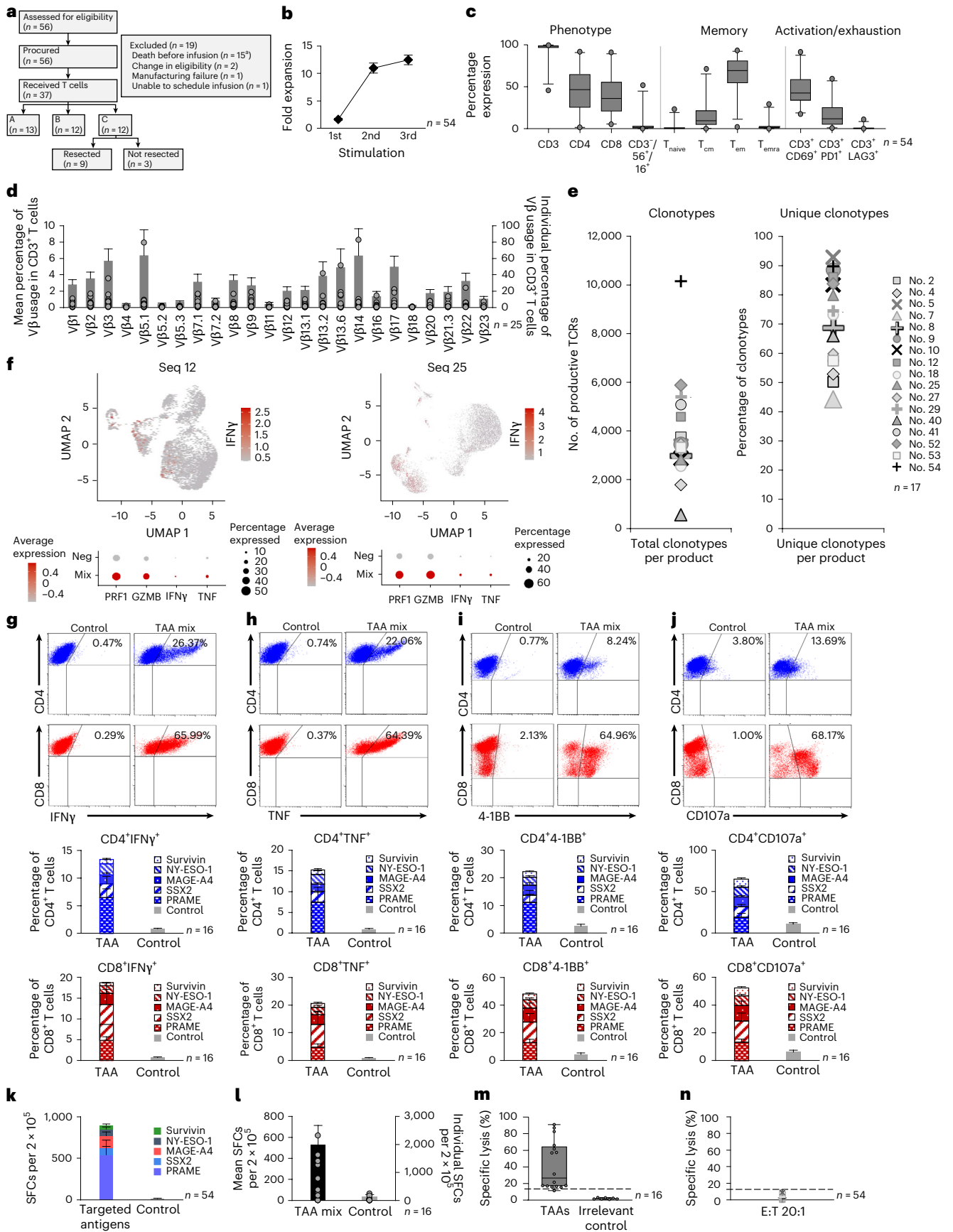


**Table 1 | Patient demographics (n=37)**

Characteristics	Arm A	Arm B	Arm C	All patients
	(n=13)	(n=12)	(n=12)	(n=37)
Age on study, years				
Median, range (minimum to maximum)	64.0 (42.0–85.0)	51.5 (30.0–78.0)	65.0 (43.0–78.0)	63.0 (30.0–85.0)
Sex, no. (%)				
Female to male	6/7 (46.2/53.8)	6/6 (50.0/50.0)	7/5 (58.3/41.7)	19/18 (51.4/48.6)
Race, no. (%)				
White	11 (84.6)	10 (83.3)	11 (91.7)	32 (86.5)
Black or African American	2 (15.4)	0 (0)	0 (0)	2 (5.4)
Asian	0 (0)	1 (8.3)	0 (0)	1 (2.7)
Native Hawaiian or other Pacific islander	0 (0)	1 (8.3)	0 (0)	1 (2.7)
Unknown	0 (0)	0 (0)	1 (8.3)	1 (2.7)
Ethnicity, no. (%)				
Hispanic or Latino	2 (15.4)	2 (16.7)	2 (16.7)	6 (16.2)
Non-Hispanic	11 (84.6)	10 (83.3)	9 (75.0)	30 (81.1)
Unknown	0 (0)	0 (0)	1 (8.3)	1 (2.7)
Stage, no. (%)				
I	0 (0)	0 (0)	0 (0)	0 (0)
II	0 (0)	0 (0)	12 (100.0)	12 (32.4)
III	2 (15.4)	2 (16.7)	0 (0.0)	4 (10.8)
IV	11 (84.6)	10 (83.3)	0 (0.0)	21 (56.8)

capacity (*CCR5*, *CX3CR1*, *CXCR6* and *CCL4*), inflammation or  $T_H1$  cell polarization (*E2F2*, *ADGRG1*, *IL32* and *LTB*)<sup>37–45</sup> and cytolytic activity (*NCR3*, *NKG7* and *GZM*)<sup>46–49</sup>, and downregulated genes included those linked to T cell exhaustion or impaired function (*SLC3A2*, *RGS16*, *PYCRL1*, *PSAT1* and *VLDR-ASI*)<sup>50–56</sup>. To address mTAA product potency, transcriptional profiling was combined with functional studies. Figure 1f shows data for two donors (Supplementary Fig. 2: data from five additional donors), in whom stimulation with tumor-spanning pepmixes identified a population of T cells transcribing genes for  $T_H1$  cell effector molecules including interferon- $\gamma$  (IFN $\gamma$ ), tumor necrosis factor (TNF), granzyme B (GZMB) and perforin. These results were assessed at the protein level, confirming the presence of reactive IFN $\gamma$ -producing and TNF-producing T cells in both the CD4<sup>+</sup> and CD8<sup>+</sup> subsets (Fig. 1g,h, top: representative intracellular cytokine staining (ICS) IFN $\gamma$  results; bottom: summary results) (13.4  $\pm$  4.3%: CD4; 18.7  $\pm$  8.0%: CD8<sup>+</sup>, TNF; 15.3  $\pm$  4.8%: CD4; 20.6  $\pm$  8.2%: CD8<sup>+</sup>). The mTAA T cells also upregulated 4-1BB (22.3  $\pm$  6.4%: CD4; 48.1  $\pm$  14.5%: CD8<sup>+</sup>), CD107a (64.9  $\pm$  12.7%: CD4; 52.5  $\pm$  13.2%: CD8<sup>+</sup>) and CD40L (22.9  $\pm$  6.0%: CD4) on antigen exposure (Fig. 1i,j and Supplementary Fig. 3; n = 16). For five mTAA products for which both TCR deep sequencing and scRNA-seq data were available, the functional profile of clonotypes unique to the product infused was investigated by evaluating IFN $\gamma$ , TNF, GZMB and perforin transcripts, which revealed that most (median 79.7%; range, 60.3–88.9%) exhibited an effector profile (Supplementary Fig. 4). Overall, of the stimulating antigens, PRAME induced the strongest activity (541  $\pm$  176 IFN $\gamma$  spot-forming cells (SFCs) per  $2 \times 10^5$  cells), followed in descending order by MAGEA4 (151  $\pm$  46 SFCs), NY-ESO-1 (81  $\pm$  25 SFCs), SSSX2 (78  $\pm$  22 SFCs) and Survivin (42  $\pm$  22 SFCs) (Fig. 1k). The cytotoxic potential of the mTAA products was evaluated by assessing granzyme B production (531  $\pm$  182 SFCs per  $2 \times 10^5$ ; Fig. 1l) and direct cytolytic activity against antigen-loaded targets (Fig. 1m). Finally, to assess the potential for ‘off-tumor’ effects, cytotoxicity against autologous phytohemagglutinin (PHA)-stimulated blasts was measured. As shown in Fig. 1n, there was no autoreactivity against nonmalignant cells (mean 3.0  $\pm$  0.5% specific lysis; effector-to-target (E-to-T) ratio, 20:1; n = 54),

with <10% specific lysis at an E-to-T ratio of 20:1 set as a study release criterion, which was met by all products.

#### Clinical trial primary endpoints: feasibility and safety

Supplementary Table 2 summarizes the cell dose production and infusion data for each participant and study arm.

**Production.** Among the 37 infused patients, a median of 12 cell doses per participant (range 2–28) was produced and available for infusion. Only 3 (8%) participants (patient no. 2 in arm A and patient nos. 10 and 54 in arm C) had fewer than 6 available doses, attesting to the feasibility of producing 6 doses, even from participants who were heavily pre-treated and/or actively receiving chemotherapy.

**Infusion.** Per protocol, the feasibility of completing six infusions (that is, a series) was evaluated in each arm. If two or more of the first six participants in each arm were unable to complete a series, the strategy was determined unfeasible but study enrollment continued. By this definition, it was not feasible to complete the infusion series in any of the study arms. However, reasons for stopping T cell therapy were primarily related to disease progression (n = 14), surgical complications (n = 4) or cancer-unrelated death (n = 1) (86% of cases), rather than insufficient cells, inability to administer cells or infusion-related toxicity. Patients in arm A received a median of 6 infusions (range 2–6), those in arm B a median of 2.5 infusions (range 1–6) and those in arm C a median of 3 infusions (range 1–6).

**Safety.** The 37 treated participants received a total of 140 infusions. No autoimmunity, cytokine release syndrome (CRS) or neurotoxicity was documented (Table 2 and Supplementary Table 3). Overall, 24 (64.9%) patients experienced adverse events (AEs) attributed as at least possibly related to mTAA infusions (Table 2), with only one of these being serious—a grade 3 lipase elevation classified as a treatment-related serious AE (tSAE), which occurred 3 d after the fifth T cell infusion of patient no. 11. This patient was admitted and treated for presumed

**Table 2 | Possibly treatment-related AEs by study arm and grade**

Events	Participants, no. (%)					
	Arm A (n=13)		Arm B (n=12)		Arm C (n=12)	
	Grade 1–2	Grade ≥3	Grade 1–2	Grade ≥3	Grade 1–2	Grade ≥3
Aspartate aminotransferase increased	5 (38.5)	0 (0)	1 (8.3)	0 (0)	2 (16.7)	0 (0)
Alanine aminotransferase increased	3 (23.1)	0 (0)	1 (8.3)	0 (0)	3 (25.0)	0 (0)
Fatigue	3 (23.1)	0 (0)	3 (25.0)	0 (0)	0 (0)	0 (0)
Anemia	2 (15.4)	0 (0)	1 (8.3)	0 (0)	2 (16.7)	0 (0)
Fever	1 (7.7)	0 (0)	3 (25.0)	0 (0)	0 (0)	0 (0)
Alkaline phosphatase increased	1 (7.7)	0 (0)	2 (16.7)	0 (0)	1 (8.3)	0 (0)
White blood cell decreased	2 (15.4)	0 (0)	1 (8.3)	0 (0)	1 (8.3)	0 (0)
Hypocalcemia	2 (15.4)	0 (0)	0 (0)	0 (0)	1 (8.3)	0 (0)
Chills	2 (15.4)	0 (0)	0 (0)	0 (0)	0 (0)	0 (0)
Flu-like symptoms	1 (7.7)	0 (0)	1 (8.3)	0 (0)	0 (0)	0 (0)
Body aches	0 (0)	0 (0)	2 (16.7)	0 (0)	0 (0)	0 (0)
Blood bilirubin increased	1 (7.7)	0 (0)	0 (0)	0 (0)	1 (8.3)	0 (0)
Platelet count decreased	1 (7.7)	0 (0)	1 (8.3)	0 (0)	0 (0)	0 (0)
Anorexia	1 (7.7)	0 (0)	0 (0.0)	0 (0)	1 (8.3)	0 (0)
Hypokalemia	1 (7.7)	0 (0)	1 (8.3)	0 (0)	0 (0)	0 (0)
Rash, maculopapular	1 (7.7)	0 (0)	1 (8.3)	0 (0)	0 (0.0)	0 (0)
Hypertension	1 (7.7)	0 (0)	0 (0)	0 (0)	1 (8.3)	0 (0)
Sinus tachycardia	1 (7.7)	0 (0)	0 (0.0)	0 (0)	0 (0.0)	0 (0)
Abdominal pain	0 (0)	0 (0)	1 (8.3)	0 (0)	0 (0)	0 (0)
Diarrhea	0 (0)	0 (0)	0 (0)	0 (0)	1 (8.3)	0 (0)
Dry mouth	1 (7.7)	0 (0)	0 (0)	0 (0)	0 (0)	0 (0)
Nausea	0 (0)	0 (0)	0 (0)	0 (0)	1 (8.3)	0 (0)
Creatinine increased	0 (0)	0 (0)	0 (0)	0 (0)	1 (8.3)	0 (0)
Lipase increased	0 (0)	0 (0)	0 (0)	1 (8.3)	0 (0)	0 (0)
Lymphocyte count decreased	0 (0)	0 (0)	0 (0)	0 (0)	1 (8.3)	0 (0)
Serum amylase increased	0 (0)	0 (0)	1 (8.3)	0 (0)	0 (0)	0 (0)
Hypernatremia	1 (7.7)	0 (0)	0 (0)	0 (0)	0 (0)	0 (0)
Hyponatremia	1 (7.7)	0 (0)	0 (0)	0 (0)	0 (0)	0 (0)
Arthralgia	1 (7.7)	0 (0)	0 (0)	0 (0)	0 (0)	0 (0)
Musculoskeletal and connective tissue disorder: other, specify: joint pain	1 (7.7)	0 (0)	0 (0)	0 (0)	0 (0)	0 (0)
Myalgia	1 (7.7)	0 (0)	0 (0)	0 (0)	0 (0)	0 (0)
Dysgeusia	0 (0.0)	0 (0)	1 (8.3)	0 (0)	0 (0)	0 (0)
Cough	1 (7.7)	0 (0)	0 (0)	0 (0)	0 (0)	0 (0)
Dyspnea	1 (7.7)	0 (0)	0 (0)	0 (0)	0 (0)	0 (0)
Hot flashes	1 (7.7)	0 (0)	0 (0)	0 (0)	0 (0)	0 (0)

pancreatitis and discharged within 24 h with no further symptoms, and proceeded to receive the sixth scheduled infusion with no further AEs.

### Clinical outcomes

**Arm A.** Clinical outcomes are summarized in Fig. 2a, Supplementary Table 4 and Extended Data Table 2. The best response rate after at least one infusion was 1 complete response (CR) (7.7%), 2 partial responses (PRs) (15.4%), 8 stable disease (SD) (61.5%) and progressive disease (PD) in 2 patients (15.4%), for an overall response rate (ORR) of 23.1% (95% confidence interval (CI): 5.0–53.8%) and disease control rate (DCR) of 84.6% (95% CI: 54.6–98.1%). The three arm A responders had SD before

study entry (Extended Data Table 2). The median duration of response (DOR) for those who achieved a PR or CR was 7.5 months (range 3.5–16.6 months), whereas a median duration of control (DOC) for patients with CR, PR or SD was 6.3 months (range 0.7–16.6 months). The median event-free survival (EFS) and overall survival (OS) for arm A participants were 6.4 months (95% CI: 2.4–9.5 months) and 14.1 months (95% CI: 3.6–15.4 months), respectively (Fig. 2d,e and Supplementary Table 5).

**Arm B.** Clinical outcomes are summarized in Fig. 2b, Supplementary Table 4 and Extended Data Table 2. No objective responses were

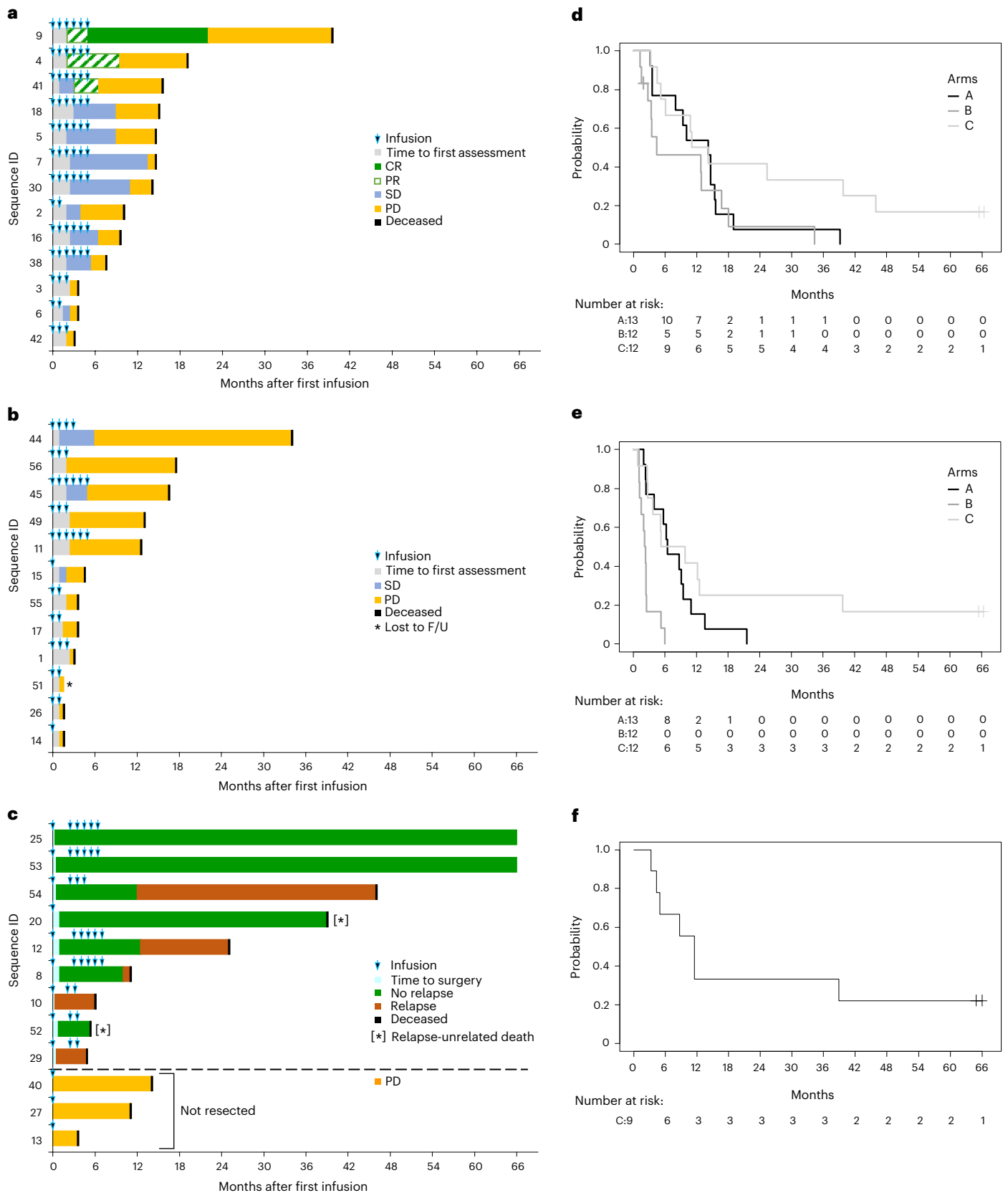
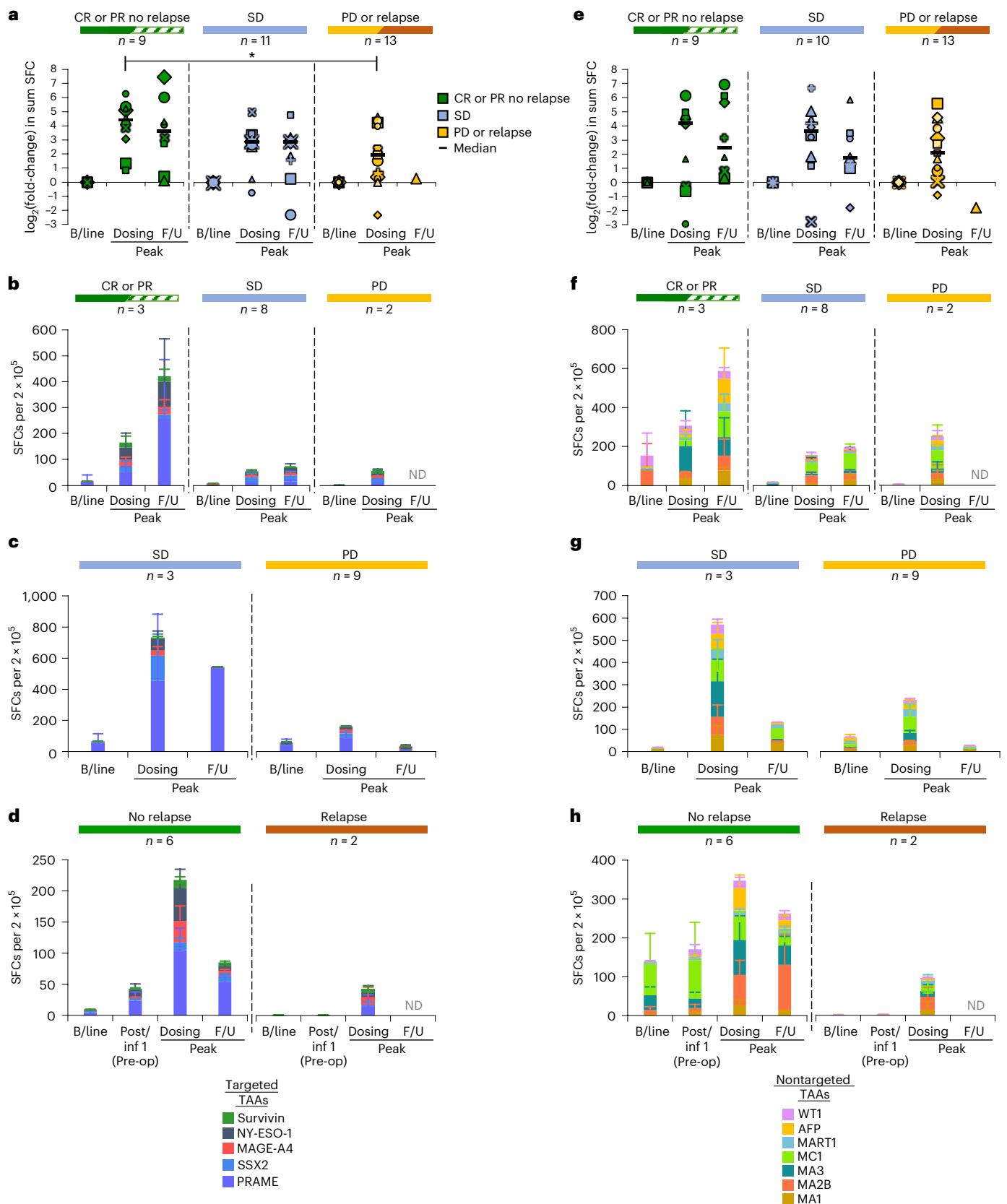


**Fig. 2 | Clinical outcomes.** a–c, Swimmers’ plots depicting DORs after mTAA infusions in patients treated in arms A (a), B (b) and C (c). The timing of infusions is indicated. d–f, Kaplan–Meier survival analysis. Survival estimates are shown

for OS (d, all arms;  $n = 37$ ), EFS (e, all arms;  $n = 37$ ) and RFS (f; arm C only, resected patients;  $n = 9$ ). F/U, follow-up, between 1 month and 12 months after the last infusion.



recorded. Three patients (25%) had a best response of SD and the remaining nine patients (75%) had PD, for an ORR of 0% and DCR of 25.0% (95% CI: 5.5–57.2%). The median EFS and OS were 2.2 months (95% CI: 1.2–2.5 months) and 4.4 months (95% CI: 1.5–16.7 months), respectively (Fig. 2d,e and Supplementary Table 5).

**Arm C.** Clinical outcomes are summarized in Fig. 2c and Extended Data Table 2. Nine (75%) participants proceeded to planned resection whereas three (25%) were found to have unresectable or metastatic disease at the time of surgery. Survival estimates for OS, EFS and relapse-free survival (RFS) are shown in Fig. 2d–f and

**Fig. 3 | In vivo T cell activity.** **a, e**, in vivo expansion of tumor-reactive T cells: expansion of T cells specific for targeted (**a**) and nontargeted (**e**) TAAs in patients from all three arms grouped in responders (CR, PR or no relapse) versus SD versus nonresponders (PD or relapse). Results are reported as log transformed (fold-change) in SFCs at the specified time points in relation to baseline. Each symbol represents an individual patient and median values are indicated. Statistical significance was assessed using a two-sided Student's *t*-test for continuous variables. Given the exploratory nature of the immune correlative analysis, no adjustments for multiple comparisons were made. \*Denotes statistical significance ( $P = 0.027$ ). **b–d, f–h**, In vivo behavior of circulating tumor-reactive T cells specific for both targeted (**b–d**) and nontargeted (**f–h**) TAAs in patients

treated in arms A (**b** and **f**), B (**c** and **g**) and C (**d** and **h**), respectively, grouped into responders (CR or PR) versus SD versus PD (arms A and B) and in relapsed versus nonrelapsed patients (arm C). The results are reported as SFCs (mean  $\pm$  s.e.m.) per  $2 \times 10^5$  cells at specified time points. Immune correlative analysis does not include arm C patient nos. 13, 27 and 40, who were not resected and were thus deemed nonevaluable for further analysis per study protocol, and patient no. 20 who only received a single infusion due to postsurgical complications and was deemed nonevaluable. B/line, baseline; B/line, pre-infusion 1: dosing period, during the active infusion period and up to week 4 after the last infusion; ND, no data; peak (dosing or F/U), maximum detected SFCs during the specified period; pre-op, preoperative (arm C only).

Supplementary Table 5. After 66 months of follow-up, two of the nine resected participants remained alive and disease free, despite being relatively high risk. Patient no. 25's pathological stage was ypT2N1 despite having received 4–5 months of neoadjuvant FOLFIRINOX and no adjuvant chemotherapy postsurgery. Similarly, patient no. 53 was borderline resectable at diagnosis with radiographic evidence of extensive lymphatic spread (cT2N2), and despite this remains cancer free. The median EFS and OS for all participants enrolled in arm C were 7.5 months (95% CI: 2.6–39.7 months) and 12.6 months (95% CI: 4.5–45.9 months), respectively, whereas the median RFS and OS for those who underwent resection were 11.5 months (95% CI: 3.3 months to not available (NA)) and 25.3 months (95% CI: 4.5 months to NA), respectively.

When examining all patients across all study arms, those who received more infusions appeared to do better than those who received fewer (5–6 infusions > 3–4 infusions > 1–2 infusions; Supplementary Fig 5). However, per the clinical protocol, evidence of progression precluded continuing with infusions, thus confounding this analysis.

### In vivo T cell behavior

To assess the potential contribution of our autologous, nonengineered, mTAA T cell therapy to clinical outcome, we evaluated in vivo persistence and investigated whether T cells were able to infiltrate the tumor (arm C participants). We also assessed whether there was an immune signature associated with superior clinical outcomes. To this end, we examined (1) the entire cohort (that is, all patients and all study arms) and (2) each study arm individually, dividing participants into: 'responders' (defined as those with an objective response in arm A and no relapse in arm C), those with SD (arms A and B) and 'nonresponders' (defined as PD in arms A and B and relapse in arm C). Persistence was evaluated by TCR deep sequencing analysis of peripheral blood samples collected during and after dosing to look for the presence of product-derived unique clones, whereas the expansion and functional capacity of tumor-reactive T cells were interrogated by performing IFN $\gamma$  ELISpot analysis. In addition to evaluating activity against mTAA-targeted antigens, the emergence of T cell responses directed against tumor-expressed antigens not targeted by the infused product was also assessed as an indicator of in vivo antigen spreading.

To first evaluate persistence, TCR deep sequencing was performed on select blood samples collected during dosing and follow-up in

a subset of patients ( $n = 14$ ). Extended Data Fig. 1a shows the summary results, whereas individual ribbon plots depicting circulating product-derived unique clonotypes, during both the infusion period and the 12 months of follow-up, are shown in Extended Data Fig. 1b–o. In all 14 donors analyzed, product-derived clonotypes were detected at all timepoints tested, confirming that the infused autologous, non-engineered mTAA T cells persisted in vivo. To next evaluate the infiltrative capacity of the infused T cells, tumor material from seven of nine surgically resected arm C participants was evaluated. As shown in Extended Data Fig. 2, tumor-resident T cells were detected by flow cytometry in all seven cases and the presence of line-derived unique clones was confirmed by deep sequencing.

Finally, to examine the quality and longevity of immune activity in participants who responded to therapy compared to nonresponders and those with SD, the frequency of T cells directed against our five target TAAs was evaluated in the three patient groups. Figure 3a shows the results for the entire cohort depicting the peak frequency of reactive cells detected during dosing and follow-up, whereas Extended Data Fig. 3a shows reactive T cells after each infusion, relative to baseline. The results for each study arm are shown in Fig. 3b–d and individual patient data are shown in Extended Data Figs. 4–6. The initial change in the frequency of T cells directed against the five target TAAs was most pronounced in responders and continued to increase or remained persistently high with additional infusions. Overall, the magnitude of T cell activity during dosing was significantly higher in responders compared with nonresponders (mean 3.9 versus 1.9 log $_2$  (fold-change) from baseline,  $P = 0.027$ ) and remained elevated for up to 12 months after the infusions had ceased (Fig. 3a–d). In addition, antigen spreading, as evidenced by the detection of T cells directed against nontargeted, tumor-expressed antigens, was also superior in responders versus nonresponders (Fig. 3e–h, and Extended Data Fig. 3b).

Figure 4 and Extended Data Figs. 7 and 8 show individual clinical and correlative data from select arm A and C participants. Figure 4 shows results from patient no. 9 (arm A) who achieved a complete radiographic response and patient no. 25 (arm C) who remains disease free after 66 months of follow-up. In patient no. 9 (CR; Fig. 4a), the frequency of T cells specific for nontargeted and targeted antigens increased from baseline through follow-up (Fig. 4b,c). A subset of the T cells specific for targeted antigens was confirmed to be mTAA line

**Fig. 4 | Individual clinical and immune correlative data.** **a–c**, Radiographic response (**a**) and immune activity against both nontargeted (**b**) and targeted (**c**) TAAs pre-infusion and postinfusion in arm A patient no. 9 who achieved a CR after mTAA T cells. Tracking of mTAA T cell product-derived (unique) TCR clonotypes (assessed by TCR $\beta$  deep sequencing) is shown as the number of circulating unique clonotypes overlaid on IFN $\gamma$  ELISpot charts (**c**). **d**, TAA expression (PRAME, Survivin) and CD3 $^+$  T cell infiltration in the patient's tumor (with unique mTAA-derived clones representing 0.19% of total tumor T cell content as shown by TCR $\beta$  deep sequencing) confirmed by IHC staining ( $\times 20$  magnification) performed on biopsy material collected at 4 months postinfusion $^3$ . **e, f**, The polyfunctionality of circulating infused cells, as evaluated by scRNA-seq analysis and expressed as proportion of cells bearing IFN $\gamma$  and/or TNF, GRZB and perforin transcripts. **e**, Proportion of functional TAA-reactive unique clonotypes.

**f**, Multiple effector molecule production as assessed by scRNA-seq. **g–j**, immune activity against targeted (**g**) and nontargeted (**h**) TAAs pre-infusion and postinfusion, tracking (**g**) and longitudinal functionality assessment (**i** and **j**) of circulating unique clones shown for arm C patient no. 25, who remained disease free after 66 months of follow-up. **i**, Proportion of functional TAA-reactive unique clonotypes. **j**, Multiple effector molecule production as assessed by scRNA-seq. **k**, Tumor expression of PRAME and Survivin and T cell infiltration (with unique mTAA-derived clones representing 0.34% of total tumor T cell content) confirmed by IHC staining on material excised during surgery after the first infusion $^3$ . **l**, The intratumoral presence of CD3 $^+$  T cells (both CD4 $^+$  and CD8 $^+$ ) was also demonstrated by flow cytometry.  $^3$ IHC experiments were performed once on each independent patient sample. Inset scale bars: 50  $\mu$ m.



derived (based on TCR $\nu\beta$  deep sequencing) and could be detected both in the circulation (89 and 103 clones during infusion and follow-up, respectively; Fig. 4c) and in the patient's tumor (7 clones; Fig. 4d) on biopsy material collected 4 months after T cell infusion. Of note, tumor expression of two antigens targeted by the mTAA line-derived T cells, PRAME and Survivin was confirmed for this patient (Fig. 4d). To evaluate the longitudinal functionality of the infused cells, TCR deep sequencing and scRNA-seq analysis were combined, focusing on IFN $\gamma$ , TNF, GZMB and perforin transcripts. Notably, 37.1% and 34% of the line-derived (unique) clonotypes detected during infusion and follow-up were functional (Fig. 4e) and most (79% and 80%, respectively) were polyfunctional (Fig. 4f). Figure 4g–i shows similar data for patient no. 25, whereas Extended Data Fig. 7 shows data for arm A patient nos. 4, 41 and 5, who experienced partial radiographic responses (patient nos. 4 and 41) and prolonged disease stabilization (patient no. 5) after infusion of mTAA T cells. Arm C patient nos. 53, 12 and 54 are presented in Extended Data Fig. 8.

## Discussion

In this study, we evaluated the safety and feasibility of serial autologous mTAA T cell infusions in patients across all stages and therapy lines in pancreatic cancer. Generating a sufficient number of T cells for six cell infusions was feasible, even in heavily pretreated participants and infusions were well tolerated, whether administered alone or with standard PDAC-targeted chemotherapy, because only a single grade 3 tSAE (transient lipase elevation) was reported, without any cases of CRS. Although efficacy was not the primary endpoint of this trial, objective clinical responses were observed, albeit primarily in arm A, in which patients were also receiving chemotherapy. The DCR (84.6%), median DOR (7.5 months) and median OS (14.1 months) in arm A are encouraging, given that these patients had already received 3–4 months of chemotherapy before starting T cell infusions. From an immunological perspective, there was clear evidence of persistence, expansion and sustained detection of tumor antigen-specific T cells directed against targeted TAAs and nontargeted antigens (epitope spreading). Importantly, T cell responses (magnitude, breadth and function) correlated with clinical outcome.

The current cell therapy product was designed to minimize immune escape in tumors with heterogeneous antigen expression<sup>12–15</sup>. PRAME, SSX2, MAGEA4, Survivin and NY-ESO-1 were chosen as therapeutic targets based on their: (1) frequency of expression (ranging from 2–10% for NY-ESO-1 to >75% for Survivin)<sup>24,27,28,31,33–36</sup>; (2) association with risk of progression<sup>25,26,29,30,32</sup>; and (3) documented safety as immunotherapeutic targets in both hematological<sup>20–23</sup> and solid malignancies<sup>19,57</sup>. Although tumor antigen expression was not assessed before study entry, we hypothesized that targeting this combination of antigens would maximize the likelihood that at least two would be present in each patient's tumor, as was subsequently confirmed by tumor immunohistochemistry (IHC) staining for a subset of participants. Furthermore, as these mTAA T cells have a mechanism of action quite different from cytotoxic chemotherapy, we posited that these cells could be administered as either monotherapy (as in arm B of the current study) or combined with approved chemotherapy (arms A and C).

Despite the wide spectrum of tumor stages included in this trial—from potentially resectable to refractory metastatic disease—we successfully generated mTAA T cells for 54 of the 56 (96%) enrolled patients. The expanded cells exhibited a polyclonal, T<sub>H</sub>1 cell-polarized effector profile composed of CD4<sup>+</sup> (helper) and CD8<sup>+</sup> (cytotoxic) cells that expressed a mix of central and effector memory markers. After T cell infusion without prior lymphodepletion, an increase in the frequency of circulating T cells directed against the targeted antigens was detected in most infused patients, along with evidence of in vivo antigen spreading. Furthermore, these cells were polyfunctional, exhibiting a T<sub>H</sub>1 cell-polarized or cytotoxic profile on antigen encounter and were ultimately detected circulating in the bloodstream and infiltrating tumors.

This effector or T<sub>H</sub>1 cell immune signature, which characterized both the infused cells and those induced in vivo, was sustained in patients with objective radiographic responses, whereas weaker and shorter-lived immune responses correlated with disease progression. Sethna and colleagues<sup>58</sup> recently reported a similar immunological signature in patients with surgically resected PDAC who received an individualized neoantigen vaccine (prime-boost protocol) containing up to 20 human leukocyte antigen (HLA)-class I and HLA-II targets in combination with an anti-programmed death-ligand 1 antibody and 5-fluorouracil-based combination chemotherapy. At a median follow-up of 1.5 years, 8 of 16 vaccinated patients harbored high-frequency, polyfunctional, neoantigen-specific, CD8<sup>+</sup> effector T cells that correlated with delayed PDAC recurrence, a signal that persisted during the extended 3.2-year median follow-up period. Taken together, data from ref. 58 and TACTOPS underscore the potential role of long-lived, functional, tumor-directed T cells in establishing durable antitumor immunity.

Immune evasion may have contributed to tumor progression in this trial. The PDAC TME is replete with suppressive cells (for example, myeloid-derived suppressor cells, M2 macrophages and regulatory T cells)<sup>12,15,16</sup> and cytokines (for example, granulocyte colony-stimulating factor, interleukin (IL)-10, transforming growth factor- $\beta$  (TGF $\beta$ , IL-6 and IL-4)), and both the tumor cells and adjacent immune cells frequently express checkpoint molecules that promote tumor growth and survival while suppressing effector T cell function, proliferative capacity and in vivo persistence. Hence, future studies may explore lymphodepleting patients before mTAA T cells (to potentially alter the TME and improve T cell infiltration, as well as to maximize the in vivo expansion of the infused product), performing fewer mTAA infusions but with larger cell doses, continuing to dose escalate mTAA T cells<sup>57</sup> and incorporating additional target specificities, including WT1, mesothelin and hotspot neoantigens<sup>58–65</sup>. In addition, combining mTAA T cells with other immunotherapeutic strategies (for example, checkpoint inhibitors<sup>7,66</sup>, oncolytic viruses<sup>67,68</sup>, stimulatory cytokines or tumor vaccines<sup>58,59,61,62,69,70</sup>) to enhance tumor immunogenicity and overcome immune evasion can be considered. Alternatively, mTAA T cells can be genetically modified to express transgenic molecules that enhance mTAA T cell persistence, functionality and capacity to resist the suppressive TME. In fact, our group has previously explored a strategy to overcome the hostile pancreatic TME by genetically programming T cells with a transgenic inverted cytokine receptor<sup>71,72</sup> or decoy<sup>73</sup> designed to convert the impact of immunologically suppressive molecules produced by both the tumor and the stroma (IL-4 and TGF $\beta$ ) into signals that are immunostimulatory.

This small, nonrandomized study has limitations. First, the patient population was quite heterogeneous, in terms of disease stage, prior therapies and concurrent therapies. Drawing reliable conclusions about the benefits of such an immunotherapeutic approach for patients with PDAC in general or any subset of patients with PDAC is therefore difficult. Second, as there were no control arms, this study could not establish benefit over standard therapy in arms A and C or supportive care alone in arm B. However, the robust immunological signature seen in responders and the increased frequency of functional T cells detected early postinfusion and maintained thereafter is consistent with an immunological fitness that may be associated with better outcomes. Nevertheless, only a randomized trial could prove how much infused T cells contributed independently to disease response and survival.

In summary, this study demonstrates the feasibility of generating autologous mTAA T cells in patients with all stages of pancreatic cancer and the safety of infusing them for up to 6 $\times$  at 1 $\times$  10<sup>7</sup> cells m<sup>-2</sup>. This treatment was exquisitely well tolerated. Clinical outcomes correlated with peripheral expansion of mTAA-targeted T cell clones and treatment-emergent antigen spreading. Combining TAA T cells with other new immunotherapies and/or standard-of-care (SOC) chemotherapy, or possibly as a single therapeutic modality in a strategic way, warrants further investigation.

## Online content

Any methods, additional references, Nature Portfolio reporting summaries, source data, extended data, supplementary information, acknowledgements, peer review information; details of author contributions and competing interests; and statements of data and code availability are available at <https://doi.org/10.1038/s41591-025-04043-5>.

## References

- Dreyer, S. B., Beer, P., Hingorani, S. R. & Biankin, A. V. Improving outcomes of patients with pancreatic cancer. *Nat. Rev. Clin. Oncol.* **22**, 439–456 (2025).
- Hosein, A. N., Dougan, S. K., Aguirre, A. J. & Maitra, A. Translational advances in pancreatic ductal adenocarcinoma therapy. *Nat. Cancer* **3**, 272–286 (2022).
- Hu, Z. I. & O'Reilly, E. M. Therapeutic developments in pancreatic cancer. *Nat. Rev. Gastroenterol. Hepatol.* **21**, 7–24 (2024).
- Beatty, G. L. et al. Activity of mesothelin-specific chimeric antigen receptor T cells against pancreatic carcinoma metastases in a phase 1 trial. *Gastroenterology* **155**, 29–32 (2018).
- Czaplicka, A., Lachota, M., Paczek, L., Zagodzón, R. & Kaleta, B. Chimeric antigen receptor T cell therapy for pancreatic cancer: a review of current evidence. *Cells* **13**, 101 (2024).
- Drougkas, K. et al. CAR-T Cell therapy in pancreatic and biliary Tract cancers: an updated review of clinical trials. *J. Gastrointest. Cancer* **55**, 990–1003 (2024).
- Giurini, E. F., Ralph, O., Pappas, S. G. & Gupta, K. H. Looking beyond checkpoint inhibitor monotherapy: uncovering new frontiers for pancreatic cancer immunotherapy. *Mol. Cancer Ther.* **24**, 18–32 (2025).
- Haas, A. R. et al. Two cases of severe pulmonary toxicity from highly active mesothelin-directed CAR T cells. *Mol. Ther.* **31**, 2309–2325 (2023).
- Haas, A. R. et al. Phase I study of lentiviral-transduced chimeric antigen receptor-modified T cells recognizing mesothelin in advanced solid cancers. *Mol. Ther.* **27**, 1919–1929 (2019).
- Paredes-Moscocco, S. R. & Nathwani, A. C. 10 years of BiTE immunotherapy: an overview with a focus on pancreatic cancer. *Front. Oncol.* **14**, 1429330 (2024).
- Qi, C. et al. Safety and efficacy of CT041 in patients with refractory metastatic pancreatic cancer: a pooled analysis of two early-phase trials. *J. Clin. Oncol.* **42**, 2565–2577 (2024).
- Beatty, G. L., Eghbali, S. & Kim, R. Deploying immunotherapy in pancreatic cancer: defining mechanisms of response and resistance. *Am. Soc. Clin. Oncol. Educ. Book* **37**, 267–278 (2017).
- Li, K. et al. Multi-omic analyses of changes in the tumor microenvironment of pancreatic adenocarcinoma following neoadjuvant treatment with anti-PD-1 therapy. *Cancer Cell* **40**, 1374–1391 (2022).
- Ott, P. A. et al. T-cell-inflamed gene-expression profile, programmed death ligand 1 expression, and tumor mutational burden predict efficacy in patients treated with pembrolizumab across 20 cancers: KEYNOTE-028. *J. Clin. Oncol.* **37**, 318–327 (2019).
- Ramesh, R. P. G. et al. Phenotypic heterogeneity and tumor immune microenvironment directed therapeutic strategies in pancreatic ductal adenocarcinoma. *Front. Immunol.* **16**, 1573522 (2025).
- Shakiba, M. & Tuveson, D. A. Macrophages and fibroblasts as regulators of the immune response in pancreatic cancer. *Nat. Immunol.* **26**, 678–691 (2025).
- Wattenberg, M. M. et al. Systemic inflammation is a determinant of outcomes of CD40 agonist-based therapy in pancreatic cancer patients. *JCI Insight* **6**, e145389 (2021).
- Gerdemann, U. et al. Cytotoxic T lymphocytes simultaneously targeting multiple tumor-associated antigens to treat EBV negative lymphoma. *Mol. Ther.* **19**, 2258–2268 (2011).
- Hoyos, V. et al. Multi-antigen-targeted T-cell therapy to treat patients with relapsed/refractory breast cancer. *Ther. Adv. Med. Oncol.* **14**, 17588359221107113 (2022).
- Lulla, P. D. et al. Clinical effects of administering leukemia-specific donor T cells to patients with AML/MDS after allogeneic transplant. *Blood* **137**, 2585–2597 (2021).
- Lulla, P. D. et al. The safety and clinical effects of administering a multiantigen-targeted T cell therapy to patients with multiple myeloma. *Sci. Transl. Med.* **12**, eaaz3339 (2020).
- Naik, S. et al. Donor-derived multiple leukemia antigen-specific T-cell therapy to prevent relapse after transplant in patients with ALL. *Blood* **139**, 2706–2711 (2022).
- Vasileiou, S. et al. T-cell therapy for lymphoma using nonengineered multiantigen-targeted T cells is safe and produces durable clinical effects. *J. Clin. Oncol.* **39**, 1415–1425 (2021).
- Abate-Daga, D. et al. Development of a T cell receptor targeting an HLA-A\*0201 restricted epitope from the cancer-testis antigen SSX2 for adoptive immunotherapy of cancer. *PLoS ONE* **9**, e93321 (2014).
- Armstrong, D. et al. MAGE-A4 induces non-small cell lung cancer and tumor-promoting plasma cell accumulation. *Sci. Adv.* **11**, eads4227 (2025).
- Brown, M. et al. The role of survivin in the progression of pancreatic ductal adenocarcinoma (PDAC) and a novel survivin-targeted therapeutic for PDAC. *PLoS ONE* **15**, e0226917 (2020).
- Dodson, L. F., Hawkins, W. G. & Goedegebuure, P. Potential targets for pancreatic cancer immunotherapeutics. *Immunotherapy* **3**, 517–537 (2011).
- Dong, H. et al. Survivin expression and serum levels in pancreatic cancer. *World J. Surg. Oncol.* **13**, 189 (2015).
- Hoshino, I. et al. Prognostic impact of p53 and/or NY-ESO-1 autoantibody induction in patients with gastroenterological cancers. *Ann. Gastroenterol. Surg.* **4**, 275–282 (2020).
- Kami, K. et al. Survivin expression is a prognostic marker in pancreatic cancer patients. *Surgery* **136**, 443–448 (2004).
- Koido, S. et al. Current immunotherapeutic approaches in pancreatic cancer. *Clin. Dev. Immunol.* **2011**, 267539 (2011).
- Krieg, S. et al. Nuclear survivin is a prognosticator in gastroenteropancreatic neuroendocrine neoplasms: a meta-analysis. *J. Cancer Res Clin. Oncol.* **148**, 2235–2246 (2022).
- Kubo, T. et al. Immunohistological analysis of pancreatic carcinoma after vaccination with survivin 2B peptide: analysis of an autopsy series. *Cancer Sci.* **110**, 2386–2395 (2019).
- Kubuschok, B. et al. Expression of cancer testis antigens in pancreatic carcinoma cell lines, pancreatic adenocarcinoma and chronic pancreatitis. *Int. J. Cancer* **109**, 568–575 (2004).
- Schmitz-Winnenthal, F. H. et al. Potential target antigens for immunotherapy in human pancreatic cancer. *Cancer Lett.* **252**, 290–298 (2007).
- Zhou, J. X., Li, Y., Chen, S. X. & Deng, A. M. Expression and prognostic significance of cancer-testis antigens (CTA) in intrahepatic cholangiocarcinoma. *J. Exp. Clin. Cancer Res.* **30**, 2 (2011).
- Abdulrahman, Z. et al. Tumor-specific T cells support chemokine-driven spatial organization of intratumoral immune microaggregates needed for long survival. *J. Immunother. Cancer* **10**, e004346 (2022).
- DeRyckere, D. & DeGregori, J. E2F1 and E2F2 are differentially required for homeostasis-driven and antigen-induced T cell proliferation in vivo. *J. Immunol.* **175**, 647–655 (2005).
- Hsiao, C. C., Vos, E., van Gisbergen, K. & Hamann, J. The adhesion G protein-coupled receptor GPR56/ADGRG1 in cytotoxic lymphocytes. *Basic Clin. Pharmacol. Toxicol.* **133**, 286–294 (2023).
- Mustafa, N. et al. E2f2 attenuates apoptosis of activated T lymphocytes and protects from immune-mediated injury through repression of Fas and FasL. *Int. J. Mol. Sci.* **23**, 311 (2021).

41. Peng, Y. M. et al. Specific expression of GPR56 by human cytotoxic lymphocytes. *J. Leukoc. Biol.* **90**, 735–740 (2011).
42. Sanna, F. C. et al. IL-2 and TCR stimulation induce expression and secretion of IL-32beta by human T cells. *Front. Immunol.* **15**, 1437224 (2024).
43. Tian, Y. et al. Unique phenotypes and clonal expansions of human CD4 effector memory T cells re-expressing CD45RA. *Nat. Commun.* **8**, 1473 (2017).
44. Truong, K. L. et al. Killer-like receptors and GPR56 progressive expression defines cytokine production of human CD4<sup>+</sup> memory T cells. *Nat. Commun.* **10**, 2263 (2019).
45. Zhu, J. W. et al. E2F1 and E2F2 determine thresholds for antigen-induced T-cell proliferation and suppress tumorigenesis. *Mol. Cell. Biol.* **21**, 8547–8564 (2001).
46. Chen, Y. et al. Ectopic expression of NKG7 enhances CAR-T function and improves the therapeutic efficacy in liquid and solid tumors. *Pharmacol. Res.* **210**, 107506 (2024).
47. Correia, M. P. et al. Distinct human circulating NKp30<sup>+</sup>FcepsilonRI gamma<sup>+</sup>CD8<sup>+</sup> T cell population exhibiting high natural killer-like anti-tumor potential. *Proc. Natl Acad. Sci. USA* **115**, E5980–E5989 (2018).
48. Liu, J. G. et al. Characterizing the immune landscape of tumor-infiltrating lymphocytes in non-small cell lung cancer. *Genes Immun.* **26**, 229–241 (2025).
49. Mietz, J. et al. Human effector CD8<sup>+</sup> T cells with an activated and exhausted-like phenotype control tumour growth in vivo in a humanized tumour model. *EBioMedicine* **106**, 105240 (2024).
50. Ikeda, K. et al. Slc3a2 mediates branched-chain amino-acid-dependent maintenance of regulatory T cells. *Cell Rep.* **21**, 1824–1838 (2017).
51. Lin, L., Deng, L. & Bao, Y. Identifying crucial lncRNAs and mRNAs in hypoxia-induced A549 lung cancer cells and investigating their underlying mechanisms via high-throughput sequencing. *PLoS ONE* **19**, e0307954 (2024).
52. Weisshaar, N. et al. Rgs16 promotes antitumor CD8<sup>+</sup> T cell exhaustion. *Sci. Immunol.* **7**, eabh1873 (2022).
53. Xu, X. et al. Effects of PYCR1 on prognosis and immunotherapy plus tyrosine kinase inhibition responsiveness in metastatic renal cell carcinoma patients. *Neoplasia* **43**, 100919 (2023).
54. Ye, L. & Jin, W. Identification of lncRNA-associated competing endogenous RNA networks for occurrence and prognosis of gastric carcinoma. *J. Clin. Lab. Anal.* **35**, e24028 (2021).
55. Zhang, Y. et al. Bioinformatics analysis of ferroptosis-related hub genes and immunoinfiltration in myocardial ischemia/reperfusion following heart transplantation. *BMC Cardiovasc. Disord.* **25**, 16 (2025).
56. Wang, Z. et al. A micropeptide TREP encoded by lincR-PPP2R5C promotes Th2 cell differentiation by interacting with PYCR1 in allergic airway inflammation. *Allergol. Int.* **73**, 587–602 (2024).
57. Hont, A. B. et al. Immunotherapy of relapsed and refractory solid tumors with ex vivo expanded multi-tumor associated antigen specific cytotoxic T lymphocytes: a phase I study. *J. Clin. Oncol.* **37**, 2349–2359 (2019).
58. Sethna, Z. et al. RNA neoantigen vaccines prime long-lived CD8<sup>+</sup> T cells in pancreatic cancer. *Nature* **639**, 1042–1051 (2025).
59. Balachandran, V. P. et al. Identification of unique neoantigen qualities in long-term survivors of pancreatic cancer. *Nature* **551**, 512–516 (2017).
60. El Zaitouni, S. et al. Potency and safety of KRAS G12C inhibitors in solid tumors: a systematic review. *Clin. Med. Insights Oncol.* **19**, 11795549251331759 (2025).
61. Pant, S. et al. Lymph-node-targeted, mKRAS-specific amphiphile vaccine in pancreatic and colorectal cancer: the phase 1 AMPLIFY-201 trial. *Nat. Med.* **30**, 531–542 (2024).
62. Rojas, L. A. et al. Personalized RNA neoantigen vaccines stimulate T cells in pancreatic cancer. *Nature* **618**, 144–150 (2023).
63. Sobhani, N., Pittacolo, M., D'Angelo, A. & Marchegiani, G. Recent anti-KRAS(G12D) therapies: a 'possible impossibility' for pancreatic ductal adenocarcinoma. *Cancers* **17**, 704 (2025).
64. Wasko, U. N. et al. Tumour-selective activity of RAS-GTP inhibition in pancreatic cancer. *Nature* **629**, 927–936 (2024).
65. Olaoba, O. T. et al. Driver mutations in pancreatic cancer and opportunities for targeted therapy. *Cancers* **16**, 1808 (2024).
66. Zhao, K. et al. Neoadjuvant pembrolizumab enables successful downstaging and resection of borderline resectable MSI-H/dMMR pancreatic ductal adenocarcinoma: a case report and literature review. *J. Gastrointest. Cancer* **56**, 112 (2025).
67. Garcia-Carbonero, R. et al. Phase I, multicenter, open-label study of intravenous VCN-01 oncolytic adenovirus with or without nab-paclitaxel plus gemcitabine in patients with advanced solid tumors. *J. Immunother. Cancer* **10**, e003255 (2022).
68. Musher, B. L. et al. LOAd703, an oncolytic virus-based immunostimulatory gene therapy, combined with chemotherapy for unresectable or metastatic pancreatic cancer (LOKON001): results from arm 1 of a non-randomised, single-centre, phase 1/2 study. *Lancet Oncol.* **25**, 488–500 (2024).
69. Mackensen, A. et al. CLDN6-specific CAR-T cells plus amplifying RNA vaccine in relapsed or refractory solid tumors: the phase 1 BNT211-01 trial. *Nat. Med.* **29**, 2844–2853 (2023).
70. McMillan, M. T. & Soares, K. C. Advances in vaccine-based therapies for pancreatic cancer. *J. Gastrointest. Cancer* **56**, 62 (2025).
71. Mohammed, S. et al. Improving chimeric antigen receptor-modified T cell function by reversing the immunosuppressive tumor micro-environment of pancreatic cancer. *Mol. Ther.* **25**, 249–258 (2017).
72. Sukumaran, S. et al. Enhancing the potency and specificity of engineered T cells for cancer treatment. *Cancer Discov.* **8**, 972–987 (2018).
73. Bajgain, P. et al. Secreted Fas decoys enhance the antitumor activity of engineered and bystander T cells in Fas ligandexpressing solid tumors. *Cancer Immunol. Res.* **10**, 1370–1385 (2022).

**Publisher's note** Springer Nature remains neutral with regard to jurisdictional claims in published maps and institutional affiliations.

**Open Access** This article is licensed under a Creative Commons Attribution-NonCommercial-NoDerivatives 4.0 International License, which permits any non-commercial use, sharing, distribution and reproduction in any medium or format, as long as you give appropriate credit to the original author(s) and the source, provide a link to the Creative Commons licence, and indicate if you modified the licensed material. You do not have permission under this licence to share adapted material derived from this article or parts of it. The images or other third party material in this article are included in the article's Creative Commons licence, unless indicated otherwise in a credit line to the material. If material is not included in the article's Creative Commons licence and your intended use is not permitted by statutory regulation or exceeds the permitted use, you will need to obtain permission directly from the copyright holder. To view a copy of this licence, visit <http://creativecommons.org/licenses/by-nc-nd/4.0/>.

© The Author(s) 2026

<sup>1</sup>Center for Cell and Gene Therapy, Dan L Duncan Comprehensive Cancer Center, Baylor College of Medicine, Texas Children's Hospital and Houston Methodist Hospital, Houston, TX, USA. <sup>2</sup>These authors contributed equally: Benjamin L. Musher, Spyridoula Vasileiou, Brandon G. Smaglo.

✉ e-mail: [blmusher@bcm.edu](mailto:blmusher@bcm.edu); [aleen@bcm.edu](mailto:aleen@bcm.edu)

## Methods

### Inclusion and ethics

The protocol and amendments were approved by the Baylor College of Medicine (BCM) and Houston Methodist Hospital (HMH) institutional review boards (IRBs) and the study was conducted under an investigational new drug approved by the US Food and Drug Administration (protocol no. H-40378; ClinicalTrials.gov identifier: [NCT03192462](https://clinicaltrials.gov/ct2/show/study/NCT03192462)), in accordance with the principles of the Declaration of Helsinki and the International Conference on Harmonization of Good Clinical Practice guidelines.

### Study design and patient population

TACTOPS (ClinicalTrials.gov identifier: [NCT03192462](https://clinicaltrials.gov/ct2/show/study/NCT03192462)) is a nonrandomized, three-arm, single-center, phase 1/2 trial conducted at the Dan L Duncan Comprehensive Cancer Center (BCM and HMH, Houston, TX, USA) in which patients with locally advanced or metastatic PDAC (arms A and B) and potentially resectable PDAC (arm C) received up to six fixed-dose infusions of autologous mTAA T cells. The protocol and amendments were approved by the BCM and HMH IRBs and the study was conducted under an investigational new drug approved by the Food and Drug Administration in accordance with the principles of the Declaration of Helsinki and the International Conference on Harmonization Good Clinical Practice guidelines. Participants provided written informed consent and could withdraw consent to end study participation at any time.

Eligibility requirements for T cell procurement included age  $\geq 18$  years, biopsy-proven PDAC, life expectancy of  $\geq 6$  months and hemoglobin  $\geq 7.0$  g dl<sup>-1</sup>; those with serious concurrent illness or active HIV infection were excluded. Eligibility requirements for T cell infusion included age  $\geq 18$  years, measurable disease per RECIST 1.1 criteria, life expectancy of  $\geq 3$  months, Eastern Cooperative Oncology Group performance status score of  $\leq 2$  or Karnofsky score of  $\geq 50$ , hemoglobin  $\geq 7.0$  g dl<sup>-1</sup>, bilirubin  $\leq 2 \times$  the upper limit of normal, aspartate aminotransferase  $\leq 3 \times$  the upper limit of normal, creatinine  $\leq 2 \times$  the upper limit of normal for age and completion of prior antineoplastic therapy  $\geq 1$  month before T cell infusion. Those with severe concurrent infection, HIV infection, pregnancy or medical immunosuppression with corticosteroids were excluded. If deemed eligible for T cell infusion, patients were enrolled into one of three arms: (1) advanced (locally advanced unresectable or metastatic) PDAC with investigator-assessed PR or SD per RECIST v1.1 after three 28-d cycles of first-line chemotherapy (arm A); (2) advanced PDAC with PD after first-line chemotherapy or judged by the investigator to be ineligible for SOC chemotherapy (arm B); or (3) potentially resectable PDAC after completion of standard neoadjuvant therapy (chemotherapy, radiotherapy or both) (arm C).

All study participants received a maximum of six infusions of mTAA T cells at a fixed dose of  $1 \times 10^7$  cells m<sup>-2</sup> in an arm-specific schema. The infused cell dose was chosen based on past regulatory interactions and prior clinical experience, demonstrating that targeting this mix of cancer testis antigens and TAAs was well tolerated at doses of  $2 \times 10^7$  cells m<sup>-2</sup>,  $2 \times$  infusions per patient<sup>23</sup>. In the current trial we sought to increase the infused cell dose (cumulatively) through performing repetitive infusions of  $1 \times 10^7$  cells m<sup>-2</sup>,  $6 \times$  infusions. In arm A, participants received SOC treatment of either nab-paclitaxel or gemcitabine (administered in 4-week cycles: days 1, 8 and 15 of a 28-day cycle) or FOLFIRINOX (administered every 2 weeks). Given the intent to administer mTAA T cells during the 'off week' of chemotherapy (that is, week 4 of a nab-paclitaxel cycle or week 2 of a FOLFIRINOX cycle) to minimize the impact of chemotherapy on the 'fitness' of the infused cells, infusions occurred every 4 weeks starting on week 4 (the 'off' week) of the fourth 28-day chemotherapy cycle. In arm B, T cells were infused every 4 weeks as monotherapy. In arm C, T cells were infused between 1 week and 4 weeks before surgical resection, then every 4 weeks, starting at least 8 weeks after surgery to address any minimal residual disease remaining following surgical resection of the primary mass.

Toxicity was evaluated during the 4-week period after each infusion. All patients who received at least one infusion of mTAA T cells were monitored for tSAEs. AEs were graded according to the National Cancer Institute Common Terminology Criteria for Adverse Events (CTCAE) v4.0, with the exception of CRS toxicities, which were graded using the CRS grading scale (see Clinical Protocol in Supplementary Information for full details). A tSAE was defined as grade 3–4 CTCAE toxicity or grade 3–4 CRS toxicity determined to be possibly, probably or definitely related to T cells. Per protocol, treatment would be considered unsafe and patient accrual halted for a given study arm if more than one tSAE was observed. The feasibility of completing six intravenous infusions of mTAA T cells (that is, a series) was monitored separately in each study arm using a method similar to the 3 + 3 procedure. The cumulative number of successfully completed infusion series was evaluated every three patients. If at most one patient could not finish an infusion series, then three additional patients could be enrolled in that arm. If, after six patients were treated, two or more were unable to complete the infusion series, the treatment strategy would be deemed unfeasible but additional enrollments on that arm would continue.

Patients with measurable disease (that is, lesions that could be accurately measured in at least one dimension as  $>10$  mm) were assessed by RECIST 1.1 criteria to determine clinical response based on evaluations of tumor size. Imaging was performed before the first T cell infusion and every 2–3 months thereafter, per SOC radiographic monitoring. A CR was defined as the disappearance of all target lesions, a PR as a  $\geq 30\%$  decrease in the sum of the longest diameter of target lesions, PD as a  $\geq 20\%$  increase in the sum of the longest diameter of target lesions and SD as a decrease or increase in the sum of the longest diameter of target lesions that did not meet criteria for PD or PR. Blood for correlative studies was collected before the first T cell infusion, at weeks 1, 2, 4, 6 and 8 once infusions were initiated and then at months 3, 6, 9 and 12 after the last infusion. Patients were followed clinically for up to four additional years (for a total of 5 years after the final T cell infusion) to evaluate long-term disease and survival status. Tumor material was collected from seven patients in arm C who underwent surgical resection and two patients in arm A who underwent tumor biopsies while on the study. Details can be found in the full clinical protocol supplied in Supplementary Information.

### Outcomes

The primary objective of TACTOPS was to determine the safety and feasibility of completing six intravenous infusions of mTAA T cells. The secondary objectives were to determine EFS and OS and tertiary endpoints were to assess antitumor immune activity.

Toxicities were graded according to the NCI–CTCAE v4.0 and the ASTCT consensus grading for CRS and neurological toxicity. The tSAEs were defined as grade III–IV toxicities according to CTCAE or grade III–IV CRS toxicities determined to be at least possibly related to T cells.

Clinical response was assessed using RECIST v1.1 based on diagnostic imaging (computed tomography, magnetic resonance imaging or nuclear imaging) obtained before the first infusion and every 2–3 months thereafter, for up to 1 year after the last infusion.

### Generation of mTAA T cells

Monocyte-derived DCs were isolated from peripheral blood mononuclear cells by plastic adherence, loaded with pepmixes (panels of 15-mer peptides overlapping by 11 amino acids) spanning the TAAs Survivin, SSX2, MAGEA4, PRAME and NY-ESO-1 (JPT Peptide Technologies) and cocultured (1:10) with autologous peripheral blood mononuclear cells in the presence of a T<sub>H</sub>1 cell-polarizing cytokine cocktail (IL-7 (10 ng ml<sup>-1</sup>), IL-12 (10 ng ml<sup>-1</sup>), IL-15 (5 ng ml<sup>-1</sup>) and IL-6 (10 ng ml<sup>-1</sup>); R&D Systems) in T cell medium (45% Roswell Park Memorial Institute (RPMI) medium 1640 (HyClone Laboratories), 45% Click's medium (Irvine Scientific), 2 mM GlutaMAX TM-1 (Life Technologies)

and 10% human AB serum (Valley Biomedical)). From day 10, responder T cells were restimulated weekly with pepmix-pulsed DCs (1:10 DCs to T cells) in the presence of IL-15 (5 ng ml<sup>-1</sup>) or IL-2 (50 U ml<sup>-1</sup>) (Proleukin (aldesleukin), TCH) until sufficient numbers were achieved for patient infusion and requisite release testing. The manufactured T cell lines were then cryopreserved.

### The mTAA T cell characterization studies

Enzyme-linked immunospot assay (ELISpot) analysis was used to determine the frequency of T cells secreting IFN $\gamma$  and granzyme B (Mabtech, Inc.) in response to TAA pepmixes, as described previously<sup>18</sup>. For phenotypic analysis, mTAA T cells were surface stained with phycoerythrin, fluorescein isothiocyanate, peridinin chlorophyll protein, allophycocyanin-conjugated, Alexa Fluor-700-conjugated, phycoerythrin cyanin 7-conjugated, Pacific Blue-conjugated or Krome Orange-conjugated CD3 (clone SK7), CD4 (SK3), CD8 (SK1), CD56 (B159), CD16 (SJ25C1), CD62L (DREG-56), CD45RA (HI100 or 2H4), CD45RO (UCHL1), CCR7 (3D12), CD69 (L78), CD83 (HB15e), HLA-DR (L243), PD-1 (PD1.3.5) and lymphocyte activation gene-3 (cat. no. 874501) (Becton Dickinson (BD); Beckman Coulter). Control samples labeled with the appropriate isotype antibodies were included and a 'fluorescence - 1' strategy was used for multicolor staining. Cells were analyzed using FACScan equipped with a filter set for four fluorescence signals, using CellQUEST software, or FACS-Canto II, using DIVA software (BD). TCR $\beta$  flow cytometric analysis was performed using the IOTest Beta Mark kit (Beckman Coulter), as per the manufacturer's instructions. Briefly,  $0.5 \times 10^6$  cells per tube were surface stained with CD3 and the TCR $\beta$ -specific monoclonal antibodies provided with the kit and incubated for 20 min at room temperature in the dark.

Subsequently, cells were washed, resuspended in 300  $\mu$ l of phosphate-buffered saline (PBS, Sigma-Aldrich) and at least 10,000 live T cells acquired on a Gallios Flow Cytometer and analyzed with Kaluza Flow Analysis Software (Beckman Coulter).

ICS was performed by stimulating mTAA T cells with target or irrelevant (control) pepmixes in the presence of CD28 and CD49d (1  $\mu$ g ml<sup>-1</sup>), followed by the addition of BD GolgiStop and BD Golgi-Plug, which contain monensin and brefeldin A, respectively. After an overnight incubation, T cells were washed, pelleted and surface stained with CD8 and CD3, then fixed and permeabilized with Cytofix or Cytoperm solution. After manufacturer-directed incubations and washes, cells were stained with IFN $\gamma$  and TNF antibodies, then acquired (at least 50,000 live cells) using a Gallios flow cytometer and analyzed with Kaluza software. All ICS reagents were from BD. For activation-induced marker staining, T cells were incubated for 5–18 h with target TAA pepmixes along with CD28 and CD49d to detect peak expression of CD40L, CD69 and 4-1BB. Next, cells were stained at 4 °C for 20 min with saturating amounts of antibodies (5  $\mu$ l per antibody per tube: CD3, CD4, CD8, 4-1BB, CD69 and CD40L, all from BD). Subsequently, cells were washed, resuspended in PBS and data were acquired on a Gallios flow cytometer, by collection of at least 50,000 live cells, and analyzed with Kaluza software. For CD107a degranulation assays, mTAA T cells were incubated for 5–6 h with target pepmixes along with CD107a (BD), GolgiStop, CD28 and CD49d. Next, cells were washed in PBS, pelleted and surface stained with CD3, CD4 and CD8 (5  $\mu$ l per antibody per tube) for 20 min at 4 °C. Subsequently, cells were washed, resuspended in PBS, acquired on a Gallios flow cytometer (at least 50,000 live cells) and analyzed using Kaluza software. A vital dye CFSE (CellTrace CFSE Cell Proliferation Kit, Invitrogen) cytotoxicity assay was employed to evaluate the specific cytolytic activity of mTAA T cells against antigen-pulsed autologous PHA blasts (tumor reactivity) using an optimized protocol as previously described<sup>74</sup>. Cytotoxicity of each mTAA T cell line toward unpulsed autologous PHA blasts (autoreactivity) was measured in a standard 4-h <sup>51</sup>Cr release assay at varying E-to-T ratios (40:1, 20:1, 10:1 and 5:1) and the percentage of specific lysis was calculated as: ((Experimental

release – Spontaneous release)/(Maximum release – Spontaneous release)  $\times$  100.

### The mTAA T cell in vivo persistence studies

To track the infused mTAA T cells, we applied high-throughput deep sequencing of TCR $\beta$  CDR3 regions (Adaptive Biotechnologies). Deep sequencing was performed on infused mTAA T cell lines and patient peripheral blood (and tumor, when available) before and after infusion. Those T cell clones identified within the product, but not detected in the patient's blood before T cell infusion, were coded as line-derived unique clones. The TCR $\beta$  deep sequencing data are available in ImmuneACCESS (<https://doi.org/10.21417/BLMC2025NM>).

### Tumor antigen profiling

To evaluate CD3 infiltration and TAA expression, available tumor tissue slides were analyzed by IHC using a one-step staining technique. Briefly, formalin-fixed paraffin-embedded, unstained slides (4–5  $\mu$ m thickness) were stained with a clinical grade CD3 antibody to identify infiltrating T lymphocytes; to detect TAA expression, the following anti-human primary antibodies were used: MAGEA4 mouse monoclonal antibody (mAb) (clone 6C1, 1:200), NY-ESO-1 mouse mAb (clone E978, 1:50) (both Santa Cruz Biotechnology), PRAME rabbit polyclonal antibody (1:200, Bioss Antibodies), SSX2 mouse mAb (clone CL3202, 1:500; Atlas Antibodies) and Survivin rabbit mAb (clone 71G4B7, 1:500, Cell Signaling Technology). Standard deparaffinization, rehydration, heat antigen retrieval with citrate buffer, pH 6, elimination of endogenous peroxidase activity by 3% hydrogen peroxide (Thermo Fisher Scientific, cat. no. H323-500) and nonspecific normal horse serum (2.5%) block were performed with 1 $\times$  Tris-buffered saline and Tween 20 washes. The TAA-specific antibodies were applied overnight at 4 °C. The next day, an anti-mouse secondary antibody (Ready Vector Labs, cat. no. MP-7402) or anti-rabbit secondary antibody (Ready Vector Labs, cat. no. MP-7402) was applied and then 3,3'-diaminobenzidine brown substrate was added to the slides. After 2–5 min of incubation, the slides were washed with water and counterstained with hematoxylin, rinsed in deionized water, dehydrated in alcohol and cover slipped with Cytoseal 60 mounting medium. Hematoxylin and eosin-stained and unstained slides served as positive and negative controls, respectively. Testes with intact spermatogenesis and epididymis served as positive and negative tissue controls, respectively. The intensity of staining was graded as 1+ (weak), 2+ (moderate) or 3+ (strong), using the combination semiquantitative scoring method. All scoring was performed by a pathologist who was blinded to the clinical outcome as well as to the demographics of individual patients.

### ScRNA-seq

**Single-cell TCR and 5'-expression sequencing.** The mTAA T cells were thawed, rested in T cell medium and resuspended at  $2 \times 10^6$  cells ml<sup>-1</sup> and 200  $\mu$ l was added per well of a 96-well plate. The mTAA T cells were incubated overnight with either 200 ng of stimulating pepmix (PRAME, SSX2, MAGEA4, NY-ESO-1 and Survivin) or dimethyl sulfoxide alone (unstimulated control). The following day, cells were harvested and passed through a 30- $\mu$ m cell strainer and dead cells were magnetically removed (Dead Cell Removal kit, Miltenyi Biotec). The resulting single-cell suspensions ( $1 \times 10^5$  cells per 100  $\mu$ l in RPMI + 10% fetal bovine serum) were loaded on to a chromium chip and captured with barcoded gel beads at a target rate of ~5,000 cells per patient sample (10x Genomics). Barcoded and amplified complementary DNAs were used for TCRV(D)J enrichment (2  $\mu$ l of cDNA) and 5'-gene expression analysis (10  $\mu$ l of cDNA). V(D)J and 5'-expression libraries were pooled and sequenced by Illumina NovaSeq sequencer (read 1, 26 bp; index, 8 bp; read 2, 90 bp).

**Single-cell data processing.** The analysis pipelines in Cell Ranger were used for sequencing data processing. FASTQ files were generated

using cell ranger mkfastq with default parameters. Then, cell ranger count was run with transcriptome = refdata-cellranger-GRCh38-1.2.0 for each sample, in which reads had been mapped on the human genome (GRCh38/hg38) using STAR (v2.7.2a). TCR data were processed by running cell ranger vdj with reference = refdata-cellranger-VDJ-GRCh38-alts-ensembl-2.0.0 to assemble TCR  $\alpha$  and  $\beta$  chains and determine clonotypes. The Seurat R package was used to run principal components analysis,  $t$ -stochastic neighbor embedding ( $t$ -SNE) and  $k$ -means clustering algorithms to visualize clustered cells in a two-dimensional space. Principal components analysis-reduced data were passed into  $t$ -SNE, a nonlinear dimensionality reduction method. Cytokine-producing cellular subpopulations were assessed and visualized using Loupe Browser and they were matched to their respective clonotypes for the TCR  $\beta$  chains using Loupe VDJ Browser (<https://10xgenomics.com>). Those identified as  $v\beta$  CDR3 were then manually compared with the line-derived unique TCR $\beta$  CDR3 regions generated as described above by deep sequencing (Adaptive Biotechnologies). DEGs were identified for each sequenced T cell product by comparing the TAA-stimulated versus unstimulated cells; a gene expression cut-off of  $\log_2(\text{fold-change}) > 1$  or  $< -1$  and an adjusted  $P \leq 10^{-6}$  were applied to select DEGs. Functional enrichment analysis of DEGs was performed using publicly available online databases (<https://www.gsea-msigdb.org/gsea/index.jsp> and <https://biit.cs.ut.ee/gprofiler/gost>). The raw sequencing data and processed scRNA-seq expression matrices generated in this study are publicly available in the Gene Expression Omnibus (GEO) under accession no. [GSE307914](https://doi.org/10.1038/s41591-025-04043-5).

### Statistical analysis

Descriptive statistics were calculated to summarize demographics, clinical characteristics and immunological parameters using mean, s.d., s.e.m., median and range. The ORR was defined as the proportion of evaluable patients with a best response of CR or PR to T cell infusions. The DCR was defined as the proportion of evaluable patients with a best response of CR, PR or SD. ORR and DCR, which were calculated along with exact 95% binomial CIs, were assessed in patients in arms A and B but not in those in arm C (because the latter underwent surgical resection after a single T cell infusion and without any intervening radiographic imaging).

OS, EFS and RFS were calculated using the Kaplan–Meier method and summarized with median survival times and 95% CIs. OS was defined as the time from the first infusion to death from any cause, EFS as the time from the first infusion to the first occurrence of disease progression, relapse or death from any cause and RFS as the time from surgery to recurrence or death from any cause. Patients without events were censored at the last follow-up date. Data for the analyses were collected up to 14 July 2025.

Summary statistics were also calculated at pre- and postinfusion timepoints to evaluate the T cell expansion and persistence based on immunological parameters; these analyses were performed in each patient group and for all treated patients. Peak T cell expansion during dosing period and follow-up was  $\log(\text{transformed})$  to achieve normality and comparisons between groups (responders versus nonresponders, and so on) were made using the Student's  $t$ -test for continuous variables. Given the exploratory nature of the immunological component, no adjustments for multiple comparisons were made. A  $P < 0.05$  was considered statistically significant. Circos visualization was performed using shinyCircos v2.0 (ref. 75). For Sankey style data visualization (ribbon plots), HTML and JavaScript code were used leveraging the D3.js library for graphics (<https://d3js.org/>)<sup>76</sup> and Grok 3-beta (2025) for code generation and refinement (<https://x.com/i/grok>).

### Reporting summary

Further information on research design is available in the Nature Portfolio Reporting Summary linked to this article.

### Data availability

Data generated during the study are maintained in electronic format on a database housed by the Center for Cell and Gene Therapy, BCM. Clinical data are stored in our clinical trials management system (OnCore). All data used in the analysis of the findings in the present study are included in the paper and the Supplementary Information. The TCR $\beta$  deep sequencing data are available in ImmuneACCESS (<https://doi.org/10.21417/BLMC2025NM>). The raw sequencing data and processed scRNA-seq expression matrices generated in this study are publicly available in the GEO under accession no. [GSE307914](https://doi.org/10.1038/s41591-025-04043-5). All other data (raw or analyzed) are available from the corresponding authors (B.L.M. or A.M.L.) on reasonable request. Source data are provided with this paper.

### References

74. Koukoulis, K. et al. Assessment of the cytolytic potential of a multivirus-targeted T cell therapy using a vital dye-based, flow cytometric assay. *Front. Immunol.* **14**, 1299512 (2023).
75. Yu, Y., Ouyang, Y. & Yao, W. shinyCircos: an R/Shiny application for interactive creation of Circos plot. *Bioinformatics* **34**, 1229–1231 (2018).
76. Bostock, M., Ogievetsky, V. & Heer, J. D(3): data-driven documents. *IEEE Trans. Vis. Comput. Graph* **17**, 2301–2309 (2011).

### Acknowledgements

We thank W. M. Mejia for help with figure generation and manuscript formatting and K. Koukoulis for excellent technical assistance. This work was supported by a translational research award from the V Foundation (to A.M.L.), a translational research grant from the Pancreatic Cancer Action Network (to A.M.L.), National Institutes of Health (NIH) SPORE in lymphoma (grant no. 5P50CA126752), CPRIT Early Career Clinical Investigator Award (to P.D.L.) and the Dan L. Duncan Comprehensive Cancer Center for application of the shared resources from a support grant from the NIH, National Cancer Institute (NCI; grant no. P30CA125123). In addition, this project was supported by the Genomic and RNA Profiling Core at BCM with funding from the NIH S10 (grant no. 1S10OD036427) and the NIH NCI (grant no. P30CA125123) and CPRIT (grant no. RP200504) and the Single Cell Genomics Core at BCM with funding from CPRIT (grant no. RP200504) and the NIH (grant no. P30CA125123). The funders had no role in study design, data collection and analysis, decision to publish or preparation of the manuscript.

### Author contributions

A.M.L. conceptualized the study. B.L.M. and B.G.S. recruited patients and performed clinical assessments. B.L.M. and A.M.L. performed data analysis and interpretation and drafted the manuscript. S.V. participated in T cell product manufacturing and administration to patients, performed data acquisition, analysis and interpretation and drafted the manuscript. C.S.R. coordinated patient recruitment and clinical sample collection. A.W., M.K. and Y.V. participated in T cell product manufacturing and administration to patients and data acquisition. B.J.G. provided regulatory guidance. G.V.B. recruited patients. P.D.L. participated in T cell product administration to patients. H.E.H., C.M.R. and M.K.B. critically read and revised the manuscript. All other authors contributed in data acquisition and/or analysis. All authors approved the submitted version of the manuscript and all attested to the accuracy and completeness of the data and their full adherence with the study protocol.

### Competing interests

B.L.M. receives research funding from Diakonos and LOKON and has a consulting agreement with Gnubiotics. B.J.G. owns QBRegulatory Consulting, which has consulting agreements with Tessa Therapeutics, Marker Therapeutics, LOKON and AlloVir. H.E.H.

is a co-founder with equity in AlloVir and Marker Therapeutics, has served on advisory boards for Tessa Therapeutics, Kiadis, Novartis, Gilead Biosciences, Fresh Wind Biotechnologies and GSK, has share options in March Biosciences and CoRegen and received research support from Kuur Therapeutics and Tessa Therapeutics. C.M.R. and M.K.B. have stock and other ownership interests with Coya, Bluebird Bio, Tessa Therapeutics, Marker Therapeutics, AlloVir, Walking Fish, Allogene Therapeutics, Memgen, Kuur Therapeutics, Bellicum Pharmaceuticals, TScan Therapeutics, Abintus Bio and March Biosciences, consulting or advisory roles with Abintus Bio, Adaptimmune, Brooklyn Immunotherapeutic, Onk Therapeutics, Tessa Therapeutics, Memgen, Torque, Walking Fish Therapeutics, TScan Therapeutics, Marker Therapeutics and Turnstone Bio and receive research funding from Kuur Therapeutics. A.M.L. is a co-founder and equity holder for AlloVir and Marker Therapeutics and was a consultant to AlloVir. S.V. and M.K. were consultants to AlloVir. B.G.S. receives research funding from Merck and AstraZeneca and has a consulting agreement with Boehringer Ingelheim. The remaining authors declare no competing interests.

## Additional information

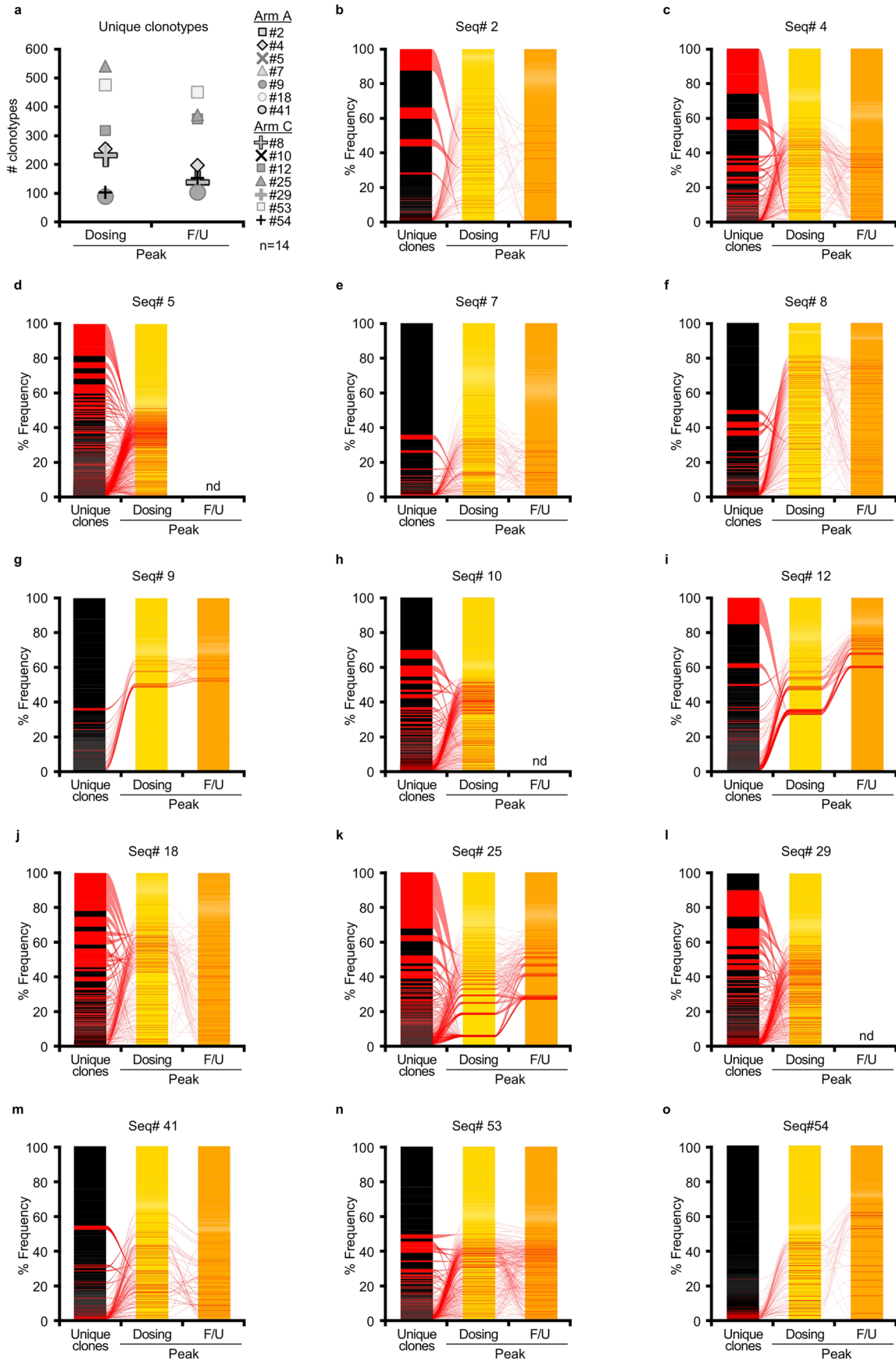
**Extended data** is available for this paper at <https://doi.org/10.1038/s41591-025-04043-5>.

**Supplementary information** The online version contains supplementary material available at <https://doi.org/10.1038/s41591-025-04043-5>.

**Correspondence and requests for materials** should be addressed to Benjamin L. Musher or Ann M. Leen.

**Peer review information** *Nature Medicine* thanks Kimberly Perez and the other, anonymous, reviewer(s) for their contribution to the peer review of this work. Peer reviewer reports are available. Primary Handling Editor: Ulrike Harjes, in collaboration with the *Nature Medicine* team.

**Reprints and permissions information** is available at [www.nature.com/reprints](http://www.nature.com/reprints).

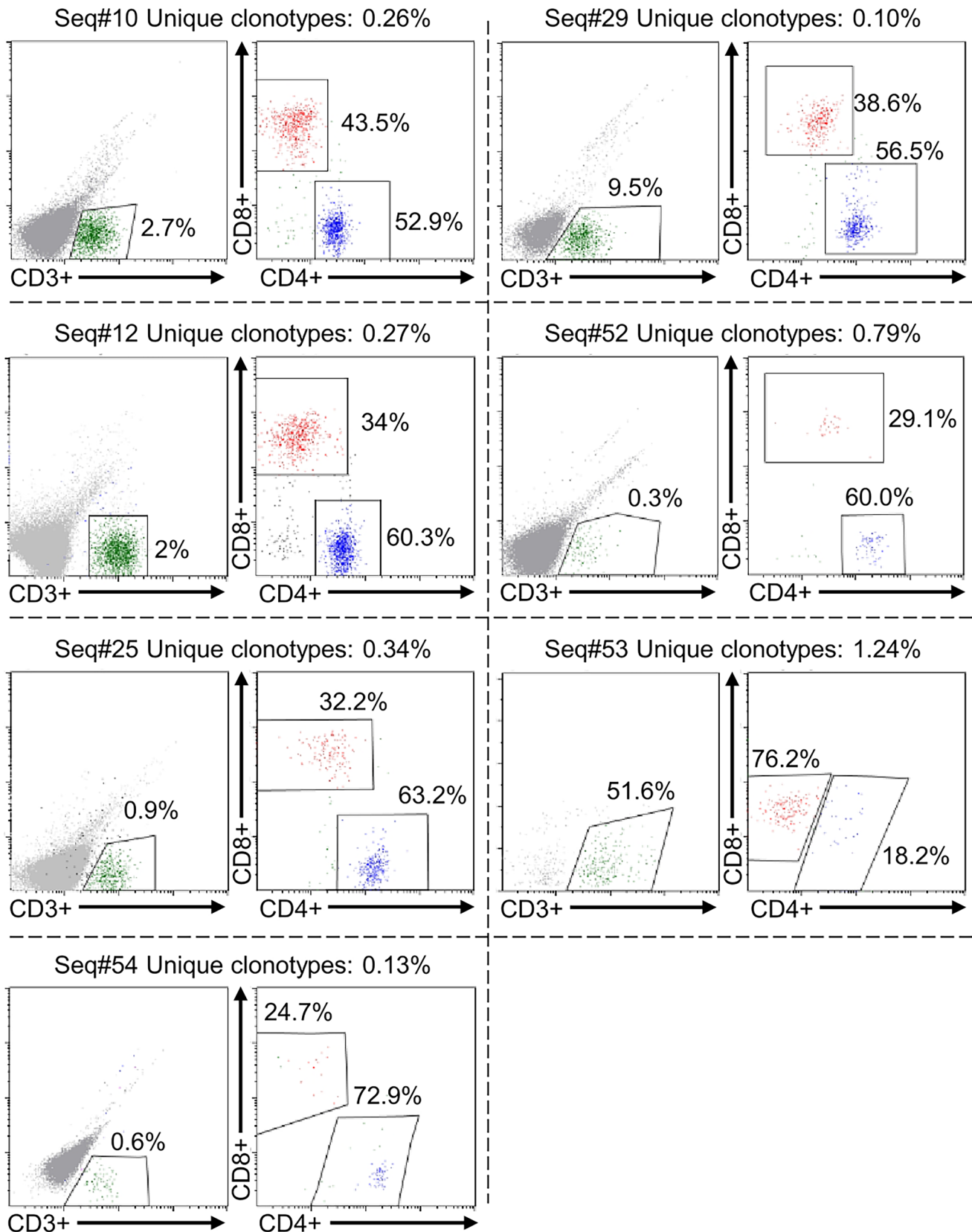


Extended Data Fig. 1 | See next page for caption.

**Extended Data Fig. 1 | Persistence of mTAA-T cells.** **a.** detection of mTAA product-derived unique clones as assessed by TCR $\beta$  deep sequencing (n = 14) both during dosing and in follow-up. Each symbol represents an individual patient. **b-o.** individual ribbon plots depicting the relative frequencies of unique clonotypes detected through dosing and in follow-up for each patient analyzed (n = 14). Each ribbon (in red) represents a single unique clonotype, while the width of the ribbon is proportional to the frequency of the clonotype in the product infused (black column) and subsequently in the patient's circulation throughout dosing (yellow column) and follow-up (orange column). **(b)** Depicts

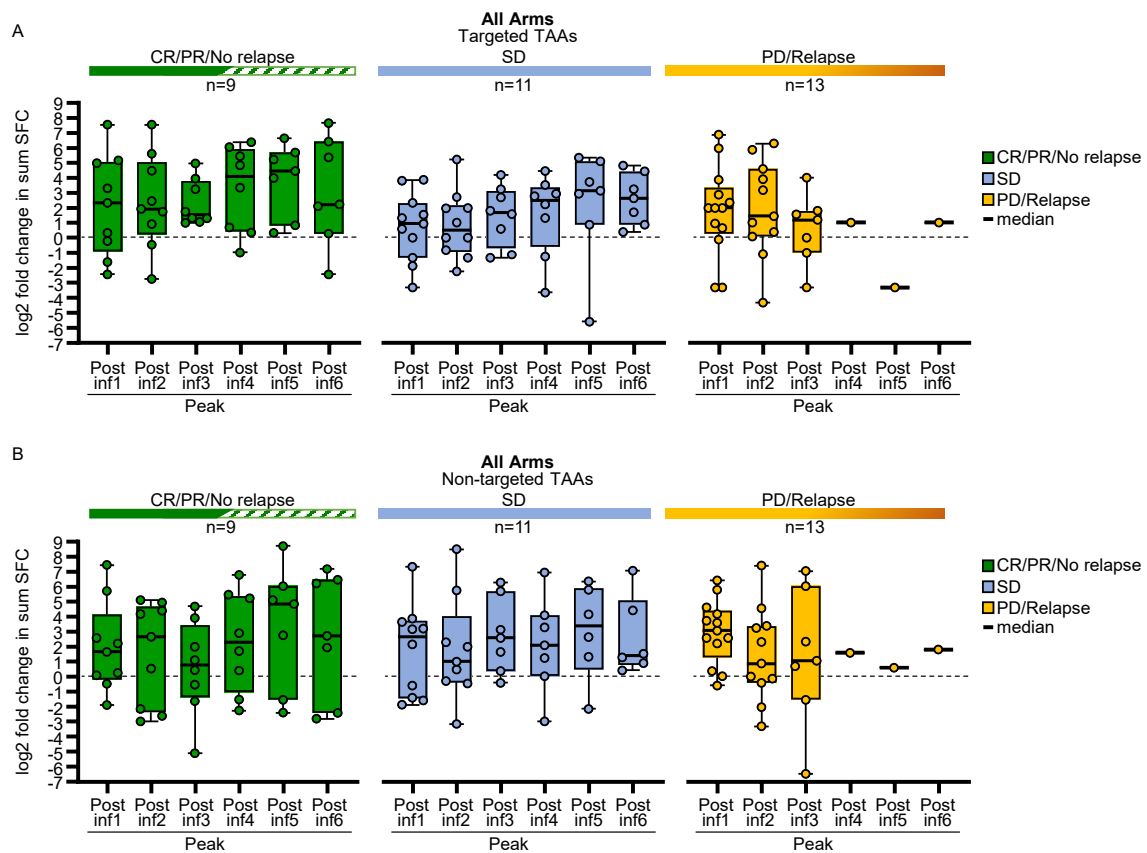
the ribbon plot data for seq #2; **(c)** depicts the ribbon plot data for seq #4; **(d)** depicts the ribbon plot data for seq #5; **(e)** depicts the ribbon plot data for seq #7; **(f)** depicts the ribbon plot data for seq #8; **(g)** depicts the ribbon plot data for seq #9; **(h)** depicts the ribbon plot data for seq #10; **(i)** depicts the ribbon plot data for seq #12; **(j)** depicts the ribbon plot data for seq #18; **(k)** depicts the ribbon plot data for seq #25; **(l)** depicts the ribbon plot data for seq #29; **(m)** depicts the ribbon plot data for seq #41; **(n)** depicts the ribbon plot data for seq #53; **(o)** depicts the ribbon plot data for seq #54.

## Detection of infiltrating T cells within tumor material



**Extended Data Fig. 2 | Detection of infiltrating T cells within tumor material.** The intratumoral presence of CD3+ T cells (both CD4+ and CD8+) was demonstrated by flow cytometry in 7 patients from Arm C for whom resected material was sent for analysis. For each seq#, percentages shown on top of the

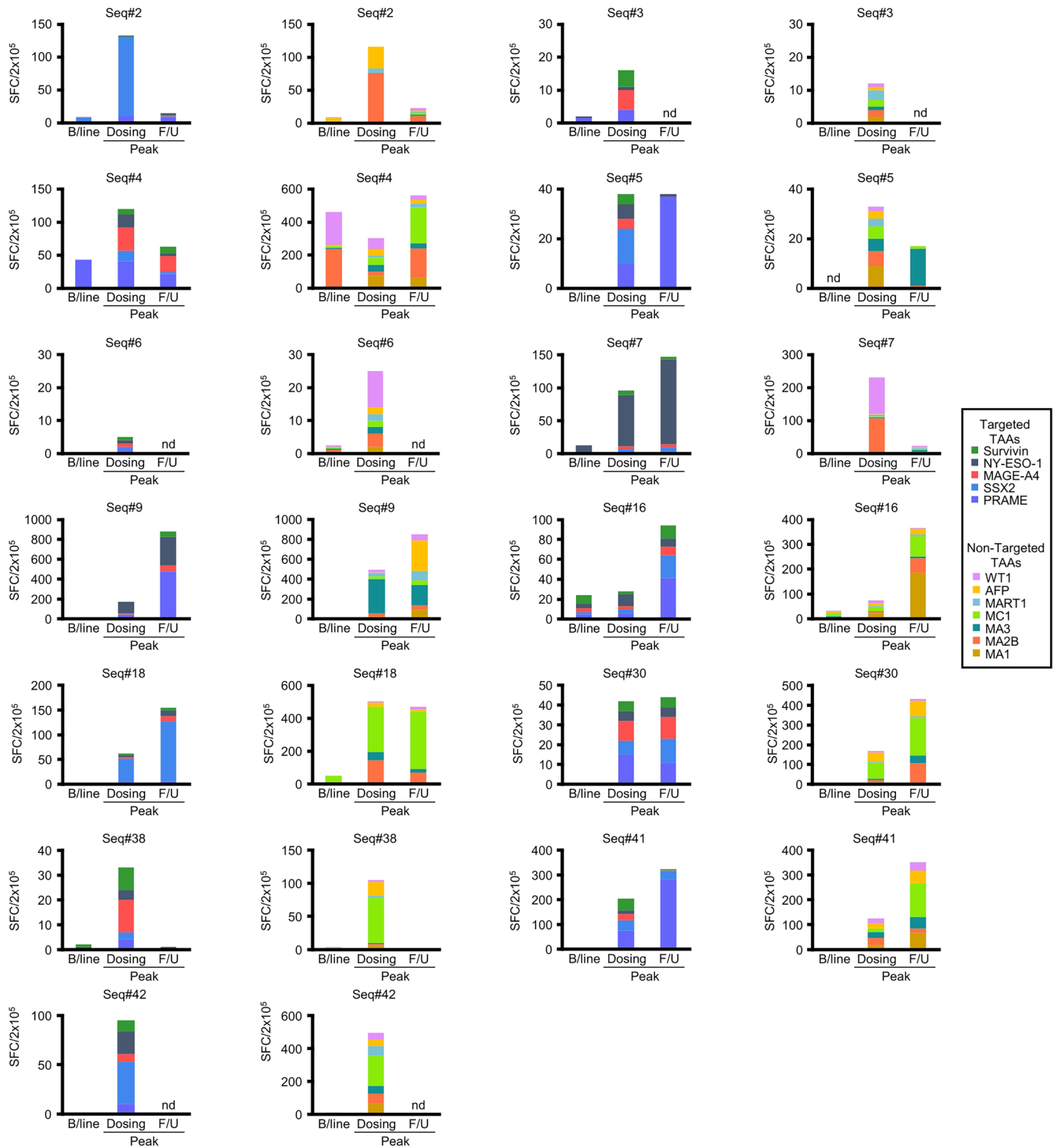
FACS plots represent the proportion of unique (mTAA line-derived) clonotypes within the total tumor T cell content as determined by TCR $\beta$  deep sequencing analysis.



**Extended Data Fig. 3 | In vivo T cell activity.** In vivo expansion of tumor-reactive T cells. Expansion of T cells specific for targeted (top - **A**) and non-targeted (bottom - **B**) TAAEs in patients from all 3 Arms grouped in responders (CR/PR/no relapse, n = 9) vs SD (n = 11) vs non-responders (PD/relapse, n = 13). Results

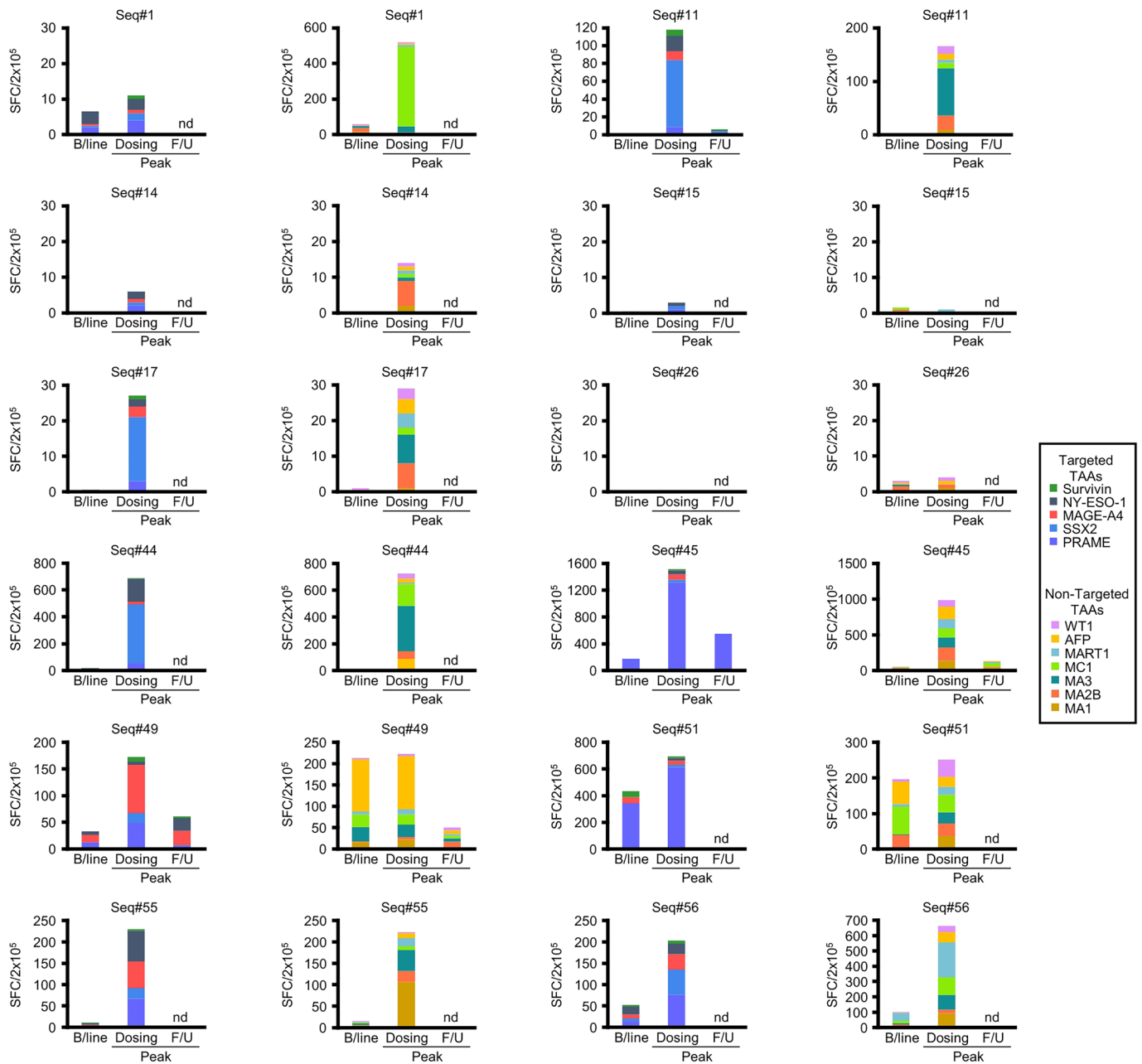
are reported as log-transformed fold change in SFC at the specified time points in relation to baseline. Box plots show median and 25th and 75th data quartiles. Whiskers extend to minima and maxima, capturing the full range of the data.

Arm A



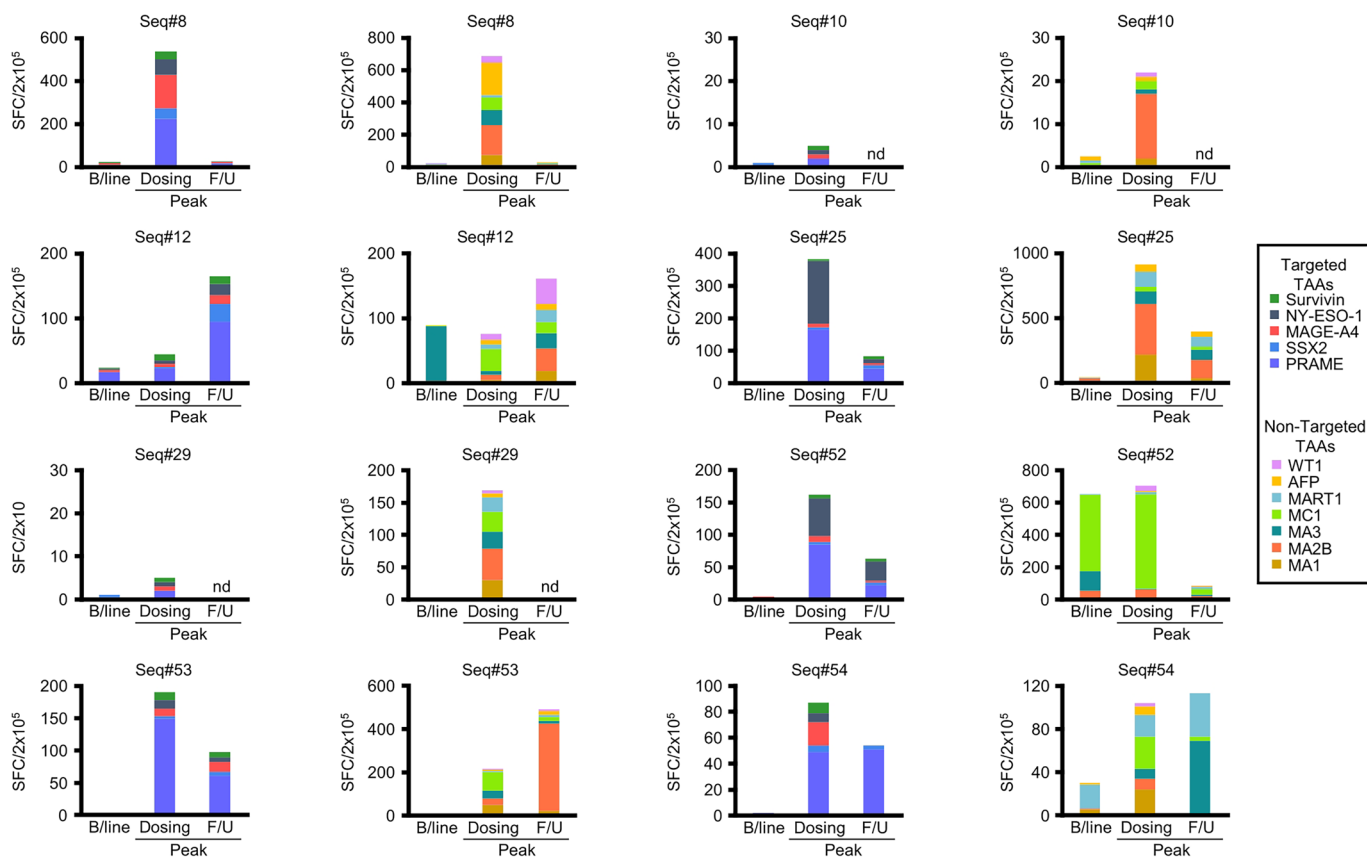
**Extended Data Fig. 4 | In vivo behavior of circulating tumor-reactive T cells—Arm A.** Trends and profile of circulating T cells specific for both targeted (left side) and non-targeted (right side) TAAs in each individual patient treated in arm A. Results are reported as SFC/2×10<sup>5</sup> at each specified time point.

Arm B



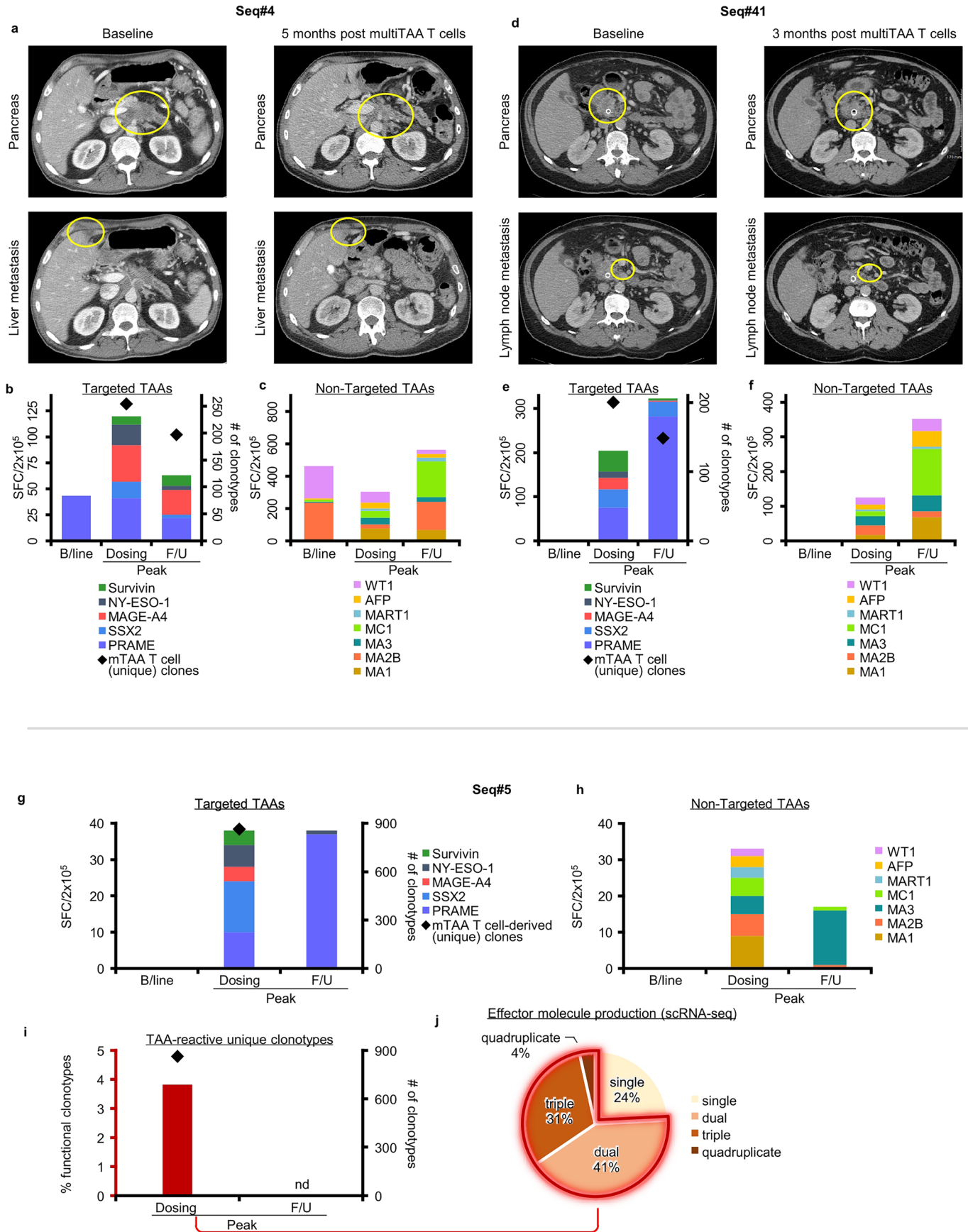
**Extended Data Fig. 5 | In vivo behavior of circulating tumor-reactive T cells—Arm B.** Trends and profile of circulating T cells specific for both targeted (left side) and non-targeted (right side) TAAs in each individual patient treated in arm B. Results are reported as SFC/2x10<sup>5</sup> at each specified time point.

Arm C



**Extended Data Fig. 6 | In vivo behavior of circulating tumor-reactive T cells - Arm C.** Trends and profile of circulating T cells specific for both targeted (left side) and non-targeted (right side) TAAs in each individual patient treated in arm C. Results are reported as SFC/2x10<sup>5</sup> at each specified time point. Arm C patients

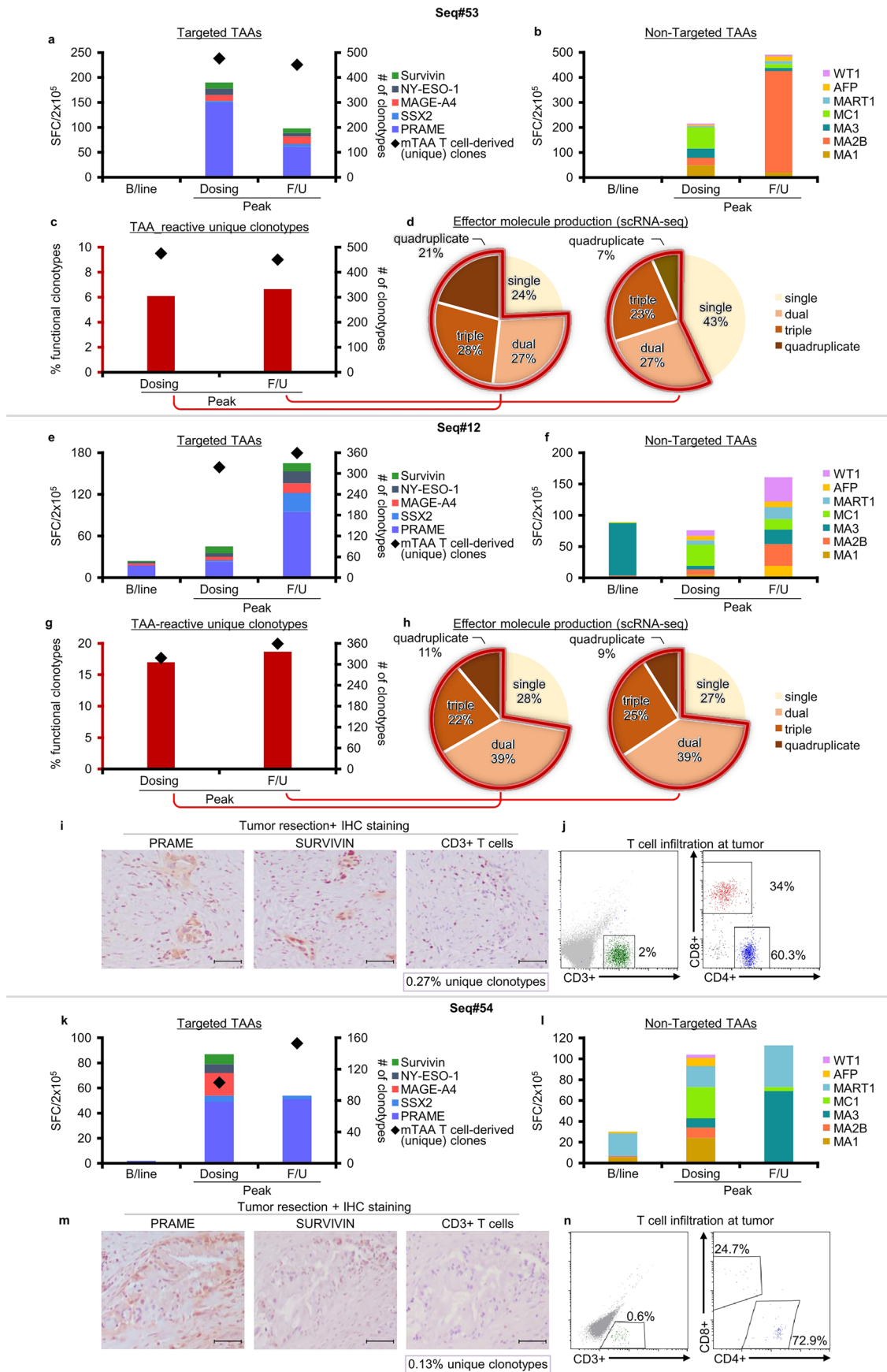
#s 13, 27 and 40 (who were not resected and were thus deemed non-evaluable for further analysis as per study protocol) and 20 (who only received a single infusion due to post-surgical complications and was deemed non-evaluable) are not included in this analysis.



Extended Data Fig. 7 | See next page for caption.

**Extended Data Fig. 7 | Individual clinical and immune correlative data – Arm A.** **a-f.** Radiographic responses (**a, d**), immune activity against targeted (**b, e**) and nontargeted (**c, f**) TAAs pre- and post-infusion and tracking (**b, e**) of circulating unique clones in patients nos 4 and 41 who achieved partial responses post-mTAA T cells. **g-j.** Immune activity against targeted (**g**) and non-targeted (**h**) TAAs pre-

and postinfusion, tracking (**g**) and functionality assessment (**i-j**) of circulating unique clones in pt no.5 who had prolonged disease stabilization following infusion. **i.** Proportion of functional TAA-reactive unique clonotypes. **j.** Multiple effector molecule production as assessed by scRNA-seq.



Extended Data Fig. 8 | See next page for caption.

**Extended Data Fig. 8 | Individual clinical and immune correlative data – Arm C. a-d.** Immune activity against targeted (a) and non-targeted (b) TAAs pre-and postinfusion, tracking (a) and longitudinal functionality assessment (c-d) of circulating unique clones in pt no.53 who remains disease-free after 66 months of follow-up. c. proportion of functional TAA-reactive unique clonotypes. d. multiple effector molecule production as assessed by scRNA-seq. e-j. Immune activity against targeted (e) and non-targeted (f) TAAs pre-and postinfusion, tracking (e) and longitudinal functionality assessment (g-h) of circulating unique clones in pt no.12 who had a prolonged relapse-free period following tumor resection. In addition, tumor expression of PRAME and Survivin and T cell infiltration (with unique mTAA-derived clones representing 0.27% of total tumor T cell content) was confirmed by IHC staining on material excised during surgery

following the first infusion\* (i). The intratumoral presence of CD3+ T cells (both CD4+ and CD8+) was also demonstrated by flow cytometry (j). k-n. immune activity against targeted (k) and non-targeted (l) TAAs pre-and postinfusion and tracking (k) of circulating unique clones in pt no.54 who remained disease-free long term post-surgery. Moreover, tumor expression of PRAME and Survivin and T cell infiltration (with unique mTAA-derived clones representing 0.13% of total tumor T cell content) was confirmed by IHC staining on material excised during surgery following the first infusion\* (m). The intratumoral presence of CD3+ T cells (both CD4+ and CD8+) was also demonstrated by flow cytometry (n). \* IHC experiments were performed once on each independent patient sample. Inset scale bars, 50µm.

Extended Data Table 1 | Patient demographics and prior or concurrent therapies

Arm	Pt ID	Age/Sex	Disease stage	Concurrent therapy	# of doses infused
A	#2	85/M	III	Gemcitabine/Paclitaxel	2
A	#3	50/F	IV	FOLFIRINOX	3
A	#4	55/M	IV	FOLFIRINOX	6
A	#5	64/F	IV	FOLFIRINOX	6
A	#6	60/F	IV	Gemcitabine/Paclitaxel	2
A	#7	72/F	IV	Gemcitabine/Paclitaxel	6
A	#9	69/F	IV	FOLFIRINOX	6
A	#16	66/M	IV	Gemcitabine/Paclitaxel	6
A	#18	42/M	III	FOLFIRINOX	6
A	#30	49/M	IV	FOLFIRINOX	6
A	#38	71/F	IV	FOLFIRINOX	6
A	#41	57/M	IV	FOLFIRINOX	6
A	#42	69/M	IV	FOLFIRINOX	3
<b>Prior therapy</b>					
B	#1	75/F	IV	Gemcitabine	3
B	#11	53/M	IV	FOLFIRINOX	6
B	#14	54/F	IV	Gemcitabine/nab-paclitaxel + LOKON (Phase 1 oncolytic virus trial)	1
B	#15	48/M	III	FOLFIRINOX + chemo/XRT	1
B	#17	64/M	IV	Gemcitabine/nab-Paclitaxel	2
B	#26	30/M	IV	FOLFIRINOX	2
B	#45	42/F	III	neoadjuvant FOLFIRINOX, gemcitabine/nab-paclitaxel once metastatic	6
B	#44	50/F	IV	FOLFIRINOX	4
B	#51	46/M	IV	adjuvant FOLFIRINOX, gemcitabine/nab-paclitaxel once metastatic	2
B	#56	35/M	IV	FOLFIRINOX -> chemo/XRT	3
B	#49	71/F	IV	FOLFIRINOX	3
B	#55	78/F	IV	FOLFIRINOX	2
<b>Neoadjuvant and/or Adjuvant Therapy</b>					
C	#8	64/F	II	FOLFIRINOX	6
C	#10	70/F	II	FOLFIRINOX	3
C	#12	63/F	II	FOLFIRINOX	6
C	#13	51/F	II	FOLFIRINOX -> chemo/XRT	1
C	#27	67/M	II	Gemcitabine/nab-Paclitaxel -> chemo/XRT	1
C	#20	78/F	II	Gemcitabine/nab-Paclitaxel	1
C	#25	63/F	II	FOLFIRINOX	6
C	#40	66/M	II	FOLFIRINOX	1
C	#29	67/M	II	Gemcitabine/nab-Paclitaxel	3
C	#53	67/M	II	FOLFIRINOX	6
C	#52	62/F	II	FOLFIRINOX -> chemo/XRT	3
C	#54	43/M	II	FOLFIRINOX	4

Extended Data Table 2 | Clinical outcomes per individual patient

Arm	Pt ID	Best disease response pre-T cells	Best disease response post-T cells	Duration of response (months)
A	#2	SD	SD	2.0
A	#3	SD	PD	NA
A	#4	SD	PR	7.5
A	#5	SD	SD	7.0
A	#6	SD	SD	1.0
A	#7	PR	SD	11.0
A	#9	SD	CR	17.0
A	#16	SD	SD	4.0
A	#18	SD	SD	6.0
A	#30	PR	SD	8.5
A	#38	SD	SD	3.5
A	#41	SD	PR	3.5
A	#42	PR	PD	NA

Arm	Pt ID	Best disease response post-T cells	Duration of response (months)
B	#1	PD	NA
B	#11	PD	NA
B	#14	PD	NA
B	#15	SD	1.0
B	#17	PD	NA
B	#26	PD	NA
B	#45	SD	3.0
B	#44	SD	5.0
B	#51	PD	Lost to f/u
B	#56	PD	NA
B	#49	PD	NA
B	#55	PD	NA

Arm	Pt ID	Best disease response post-T cells	Duration of response (months)
C	#8	No relapse	9.0
C	#10	Relapse	NA
C	#12	No relapse	11.5
C*	#13	PD	NA
C*	#27	PD	NA
C	#20	No relapse	38.0 <sup>^</sup>
C	#25	No relapse	66.0
C*	#40	PD	NA
C	#29	Relapse	NA
C	#53	No relapse	66.0
C	#52	No relapse	4.5 <sup>^</sup>
C	#54	No relapse	11.5

\*: non-resected patients; ^: relapse-unrelated death

## Reporting Summary

Nature Portfolio wishes to improve the reproducibility of the work that we publish. This form provides structure for consistency and transparency in reporting. For further information on Nature Portfolio policies, see our [Editorial Policies](#) and the [Editorial Policy Checklist](#).

### Statistics

For all statistical analyses, confirm that the following items are present in the figure legend, table legend, main text, or Methods section.

n/a Confirmed

- The exact sample size ( $n$ ) for each experimental group/condition, given as a discrete number and unit of measurement
- A statement on whether measurements were taken from distinct samples or whether the same sample was measured repeatedly
- The statistical test(s) used AND whether they are one- or two-sided  
*Only common tests should be described solely by name; describe more complex techniques in the Methods section.*
- A description of all covariates tested
- A description of any assumptions or corrections, such as tests of normality and adjustment for multiple comparisons
- A full description of the statistical parameters including central tendency (e.g. means) or other basic estimates (e.g. regression coefficient) AND variation (e.g. standard deviation) or associated estimates of uncertainty (e.g. confidence intervals)
- For null hypothesis testing, the test statistic (e.g.  $F$ ,  $t$ ,  $r$ ) with confidence intervals, effect sizes, degrees of freedom and  $P$  value noted  
*Give  $P$  values as exact values whenever suitable.*
- For Bayesian analysis, information on the choice of priors and Markov chain Monte Carlo settings
- For hierarchical and complex designs, identification of the appropriate level for tests and full reporting of outcomes
- Estimates of effect sizes (e.g. Cohen's  $d$ , Pearson's  $r$ ), indicating how they were calculated

*Our web collection on [statistics for biologists](#) contains articles on many of the points above.*

### Software and code

Policy information about [availability of computer code](#)

Data collection The clinical trial management system OnCore was used to collect individual patient case record forms.

Data analysis SAS v9.4 and R v4.4.2 were used for assessment of clinical response rates and survival rates. Descriptive statistics were used for data analysis (Microsoft Excel 2016). Kaluza Analysis v2.1 (Beckman Coulter) was used for flow cytometry data analysis. CellQUEST and DIVA (Becton Dickinson) were used for flow cytometry data analysis. Aperio ImageScope v12.4 was used for IHC slide visualization. shinyCircos v2.0 was used for circos plots generation. HTML and JavaScript code were used leveraging the D3.js library for graphics (<https://d3js.org/>) and Grok 3-beta for code generation and refinement (<https://x.com/i/grok>) for Sankey style data visualization (ribbon plots). Cell Ranger, Loupe Browser and Loupe VDJ Browser (<https://10xgenomics.com>) were used for scRNA sequencing data processing. The Seurat R package was used to run principal components analysis (PCA), t-stochastic neighbor embedding (t-SNE), and k-means clustering algorithms to visualize clustered cells in a two-dimensional space.

For manuscripts utilizing custom algorithms or software that are central to the research but not yet described in published literature, software must be made available to editors and reviewers. We strongly encourage code deposition in a community repository (e.g. GitHub). See the Nature Portfolio [guidelines for submitting code & software](#) for further information.

## Data

Policy information about [availability of data](#)

All manuscripts must include a [data availability statement](#). This statement should provide the following information, where applicable:

- Accession codes, unique identifiers, or web links for publicly available datasets
- A description of any restrictions on data availability
- For clinical datasets or third party data, please ensure that the statement adheres to our [policy](#)

Data generated during the study is maintained in electronic format on a database housed by the Center for Cell and Gene Therapy, Baylor College of Medicine. Clinical data is stored in our clinical trials management system (OnCore). All data used in the analysis of the findings in the present study are included in the manuscript and the Supplementary Information and are also provided as source data. The TCR $\beta$  deep sequencing data are available in ImmuneACCESS (DOI: 10.21417/BLMC2025NM). The raw sequencing data and processed scRNA-seq expression matrices generated in this study are publicly available in the Gene Expression Omnibus (GEO) under accession number GSE307914. All other data (raw or analyzed) are available from the corresponding authors (B.L.M. or A.M.L.) on reasonable request.

## Research involving human participants, their data, or biological material

Policy information about studies with [human participants or human data](#). See also policy information about [sex, gender \(identity/presentation\), and sexual orientation](#) and [race, ethnicity and racism](#).

Reporting on sex and gender	Sex and gender were not considered in study design since they were not relevant to the topic of the study. Overall, 19 female and 18 male subjects were treated (sex being defined based on biological attributes).
Reporting on race, ethnicity, or other socially relevant groupings	Race, ethnicity or other socially relevant groupings were not considered in study design. Based on self-reported ethnicity, 30 non-hispanic subjects, 6 hispanic and 1 subject of unknown ethnicity were treated in the study.
Population characteristics	37 treated adult patients: their characteristics are described in the manuscript and in Supplementary Materials
Recruitment	Patients were recruited based on study eligibility criteria (described in Methods and in the clinical protocol) and after informed consent (H-40378).
Ethics oversight	The protocol and amendments were approved by the Baylor College of Medicine and Houston Methodist Hospital Institutional Review Boards, and the study was conducted under an IND approved by the FDA (H-40378, NCT03192462), in accordance with the principles of the Declaration of Helsinki and the International Conference on Harmonization of Good Clinical Practice guidelines.

Note that full information on the approval of the study protocol must also be provided in the manuscript.

## Field-specific reporting

Please select the one below that is the best fit for your research. If you are not sure, read the appropriate sections before making your selection.

Life sciences       Behavioural & social sciences       Ecological, evolutionary & environmental sciences

For a reference copy of the document with all sections, see [nature.com/documents/nr-reporting-summary-flat.pdf](https://www.nature.com/documents/nr-reporting-summary-flat.pdf)

## Life sciences study design

All studies must disclose on these points even when the disclosure is negative.

Sample size	Refer to the clinical protocol for sample size estimates; in brief, the assigned sample size was 15 patients in each study Arm with the primary goal of assessing the safety and feasibility of administering 6 mTAA-T cell infusions.
Data exclusions	No data were excluded from the analysis
Replication	Experiments were performed independently on individual patient samples.
Randomization	Not relevant to this study
Blinding	Not relevant to this study

## Reporting for specific materials, systems and methods

We require information from authors about some types of materials, experimental systems and methods used in many studies. Here, indicate whether each material, system or method listed is relevant to your study. If you are not sure if a list item applies to your research, read the appropriate section before selecting a response.

## Materials & experimental systems

n/a	Involved in the study
<input type="checkbox"/>	<input checked="" type="checkbox"/> Antibodies
<input checked="" type="checkbox"/>	<input type="checkbox"/> Eukaryotic cell lines
<input checked="" type="checkbox"/>	<input type="checkbox"/> Palaeontology and archaeology
<input checked="" type="checkbox"/>	<input type="checkbox"/> Animals and other organisms
<input type="checkbox"/>	<input checked="" type="checkbox"/> Clinical data
<input checked="" type="checkbox"/>	<input type="checkbox"/> Dual use research of concern
<input checked="" type="checkbox"/>	<input type="checkbox"/> Plants

## Methods

n/a	Involved in the study
<input checked="" type="checkbox"/>	<input type="checkbox"/> ChIP-seq
<input type="checkbox"/>	<input checked="" type="checkbox"/> Flow cytometry
<input checked="" type="checkbox"/>	<input type="checkbox"/> MRI-based neuroimaging

## Antibodies

Antibodies used

Antibody /Catalog # /Vendor / Clone  
 CD3 AF 750 /A66329/ Beckman Coulter /UCHT1  
 CD4 KO /A96417 /Beckman Coulter /13B8.2  
 CD8 PB /A82791 /Beckman Coulter /B9.11  
 CD56 PE /IM2073U /Beckman Coulter /N901  
 CD16 PE /IM1238U /Beckman Coulter /3G8  
 CD62L ECD /IM2713U /Beckman Coulter /DREG56  
 CD45 RO APC /340438 /Becton Dickinson /UCHL1  
 CD197 (CCR7 ) FITC/ 561271 /Becton Dickinson /150503  
 CD69 PerCP /340548/ Becton Dickinson/ L78  
 CD279 (PD-1) FITC /557860 /Becton Dickinson /MIH4  
 CD3 PerCP /347344 /Becton Dickinson /SK7  
 CD8 APC /IM2469U /Beckman Coulter /B9.11  
 IFN-gamma FITC /340449 /Becton Dickinson/ 25723.11  
 TNFa PE /340512 /Becton Dickinson /6401.1111  
 CD137 (4-1BB) PE /555956 /Becton Dickinson /4B4-1  
 CD154 (CD40L) APC/ 648887 /Becton Dickinson /89-76  
 CD107a FITC /555800 /Becton Dickinson /H4A3  
 CD223 (LAG3) PerCP-Cy5.5/ 369312/ Biolegend /11C3C65

Validation

Validation of antibodies used in the study was performed according to Standard Operating Procedures of the GMP facility at the Center for Cell and Gene Therapy, Baylor College of Medicine. Furthermore, validation statements can be found on manufacturers' websites.

## Clinical data

Policy information about [clinical studies](#)

All manuscripts should comply with the ICMJE [guidelines for publication of clinical research](#) and a completed [CONSORT checklist](#) must be included with all submissions.

Clinical trial registration	NCT03192462
Study protocol	The full study protocol can be found in Supplementary Materials
Data collection	Collected in OnCore (as stated above), from January 21, 2018 until July 14, 2025 in Houston, Tx.
Outcomes	Specified in Methods and in the supplied clinical protocol

## Plants

Seed stocks

n/a

Novel plant genotypes

n/a

Authentication

n/a

## Flow Cytometry

### Plots

Confirm that:

- The axis labels state the marker and fluorochrome used (e.g. CD4-FITC).
- The axis scales are clearly visible. Include numbers along axes only for bottom left plot of group (a 'group' is an analysis of identical markers).
- All plots are contour plots with outliers or pseudocolor plots.
- A numerical value for number of cells or percentage (with statistics) is provided.

### Methodology

Sample preparation

Sample preparation is described in Methods.

Instrument

FACScan and FACS-Canto II (Becton Dickinson) and Gallios (Beckman Coulter)

Software

The software used to collect and analyze flow cytometry data is specified in Methods

Cell population abundance

Cell sorting was not performed. Details on number of collected events are provided in Methods (50,000 viable cells)

Gating strategy

Initial gating was performed based on FSC/SSC properties of the tested cell population. Subsequently, viable cells were selected, a CD3 gate was applied to include the CD3+ population and further subgating was performed within the CD3+ gate.

- Tick this box to confirm that a figure exemplifying the gating strategy is provided in the Supplementary Information.